MSc Dissertation

“Design optimisation for 3D printing of a biomedical implant”

December 17, 2021

Name:	Argyro Panieraki
ID Number:	2019019049
Supervisor:	Prof Nikolaos Bilalis
Course:	MSc in Product Design and Manufacturing
Department:	School of Production Engineering and Management
University:	Technical University of Crete

ΠΟΛΥΤΕΧΝΕΙΟ ΚΡΗΤΗΣ
TECHNICAL UNIVERSITY OF CRETE

This research is supported by the Technical University of Crete, and subsidised by PanCretan Endowment Fund (PEF), also known as, PanCretan Association of America (PAA), with the awarded Scholarship of Excellence (2020).

COVID-19 Addendum

This project has been affected by the ongoing pandemic in many ways. Access restrictions to buildings have prevented students from using the lab at the University and mainly training on the equipment. Although restrictions have been lifted, the project's experimental side has been severely hampered by difficulties in booking equipment and booking space. The essential 3D printing equipment, Meltio M450 3D Printer, was not used. This meant that the focus of this MSc dissertation project was more on the literature review and computational elements.

Acknowledgments

Foremost, I would like to thank Professor Bilalis Nikolaos very much for his priceless guidance and help throughout the project. Professor Stavroulakis Georgios and Professor Antoniadis Aristomenis are the following two persons I would like to thank for their invaluable teaching and participation in the exam selection board. Last but not least, I want to thank my family for their incalculable support and PanCretan Endowment Fund for funding and awarding this research.

Abstract

The present master dissertation examines the optimisation of a biomedical 3D printed implant study. The finite element method (FEM) is used to discretise the model of an implant made from a human shoulder blade (scapular). Simulations are performed using the Computer-Aided Design (CAD) software Siemens NX, specifically the NX Nastran solver. This work is intended to reduce implant mass and create a personalised geometry that considers the anatomy of the patient. Topological optimisation (TO) is employed, and Ti-6Al-4V is chosen as the implant's material. The different operating conditions, manufacturing constraints, and application of forces/loads at points where bone stress is applied are studied. Next, the design goal is established, which is to reduce the mass in order to allow tissue regeneration. The results show the distribution of the material. When the results are displayed, the redistribution of the material is visible, and then the lattice structure is added. Later, the printing simulation was conducted where the overlapping layers are simulated using the Direct Energy Deposition (DED) 3D printing method. Unfortunately, the real object was not able to be 3D printed.

Table of Contents

Table of Contents 6
Table of Figures 7
1 Introduction 9
2 Background 10
2.1 Scapulectomy 10
2.1.1 Clinical problem 10
2.1.2 Scapular Implants 11
2.2 Additive Manufacturing (AM) 12
2.2.2 Metal 3D printing technology 16
2.2.3 Aspects influencing metal 3D printing performance. 21
2.3 Optimisation Methods 23
2.3.1 Advantages of Optimisation 25
2.3.2 Topology Optimisation (TO) 25
2.3.3 Density Method 27
2.4 NX Nastran 27
2.4.1 Topological Optimasation Workflow 27
2.4.2 Solution creation 28
2.5 Convergent Modelling 29
2.6 Lattice structures 29
3 Methodology 30
3.1 CAD Geometry 30
3.2 Topological Optimisation Methodology 31
3.2.1 Materials 33
3.2.2 Mesh 34
3.2.3 Design Area 35
3.2.4 Design Constraint-Global 35
3.2.5 Manufacturing Constraint 36
3.2.6 Boundary conditions 37
3.2.7 Loads 37
3.2.8 Solve 39
4 Results and Discussion 39
4.1 Results 39
4.2 Validation 44
4.3 FEM results 46
4.4 Lattice structure 47
4.5 Discussion and Future Work 47

Bibliography 48

Table of Figures

Figure 1. Scapular implant. Taken from[11] 10
Figure 2. A) Recreated 3D scapular tumour representative. B) The virtual 3D replica of a scapular prosthesis. C) The dimensions of excised tumour and prosthesis were well fitted. D) X-ray demonstrated an appropriate shoulder representation 21 months after the operation. Taken from [25] 11
Figure 3.CAD to CAM translation flow chart 12
Figure 4. Laser sintering procedure. Taken from[51] 17
Figure 5. Electron beam melts powder utilising the speed of the electrons. Taken from [51] 18
Figure 6. Illustration of two DED systems: (A) laser combined with powder feedstock, and (B) electron beam and wire feedstock. Taken from [57] 20
Figure 7. The schematics of the DMD process. Taken from[51] 20
Figure 8. (a) Two Ti-6Al-4V brackets created of titanium alloy. (Image courtesy NASA). (b) Light-optical microscopy illustrates the comparison of the generated procedures. Taken from [59] 22
Figure 9. (a) Due to residual stress build-up, a titanium part is removed from the powder bed's build plate. (b) Cracks during the powder-bed process. Taken from [59]. 22
Figure 10. Warpage (Image courtesy of the Centre for Additive Manufacturing and Logistics at North Carolina State University).Taken from [59]. 23
Figure 11. Z-strength can be measured by the strength and stability of the internal bond between layers of a 3D printer part. Taken from [59]. 23
Figure 12. Comparative illustration of size, shape, and topology optimisation. Taken from [68] 24
Figure 13. Strut-based lattices: BCC (A), BCCZ (B), FCC (C), FCCZ (D), cubic (F), Octet-truss (G), and diamond (H). Taken from [87] 30
Figure 14. Model front view Figure 15. Model back view 30
Figure 16.Model top view Figure 17.Model right side view Figure 18.Model left side view 31
Figure 19. Studio spline Figure 20.Divide face 31
Figure 21. SOL 200 Topology Optimisation Solver Figure 22. Results bulk data 32
Figure 23. Simulation navigator with active meshing Figure 24. Simulation navigator with active solution 32
Figure 25. Manage materials section 33
Figure 26. 3D Tetrahedral Mesh Creation 34
Figure 27. Mesh trimetric view Figure 28. Mesh front view Figure 29. Mesh right side view 34
Figure 30. Mesh top view Figure 31. Mesh left side view Figure 32.Mesh back view 35
Figure 33. Optimisation area's elements assignment Figure 34.Elements of optimisation area in subscapular fossa cavity 35
Figure 35. Design Constraint Assignment 36
Figure 36.Material overhang associated with building on an angle θ. Figure 37. AM constraint 36
Figure 38. Point for base plate and base plate 'normal' vector 37
Figure 39. Fixed constraint assignment 37
Figure 40. Fixed elements for static study 37

Figure 41. Scapular cavities. Taken from [101] 38
Figure 42. Pressure load assignment Figure 43. Pressure load graphical representation 38
Figure 44. Subscapular fossa scapular cavity. Taken from[103] Figure 45.Material density results navigator 40
Figure 46. Normalised material density 41
Figure 47.Sparse Matrix Solver 43
Figure 48. Objective Function capture 43
Figure 49. Load case independent results Figure 50. Validation solution material density results 45
Figure 51. Validation solution material density results 45
Figure 52. Smoothed STL exported and opened in slicing software ‘Cura’ 45
Figure 53. Displacement results Figure 54. Stress results 46
Figure 55. Rotation results Figure 56. Reaction force results 46
Figure 57. Reaction moment results 46
Figure 58. Octahedroid lattice structure application 47

1 Introduction

The research study has started with an in-depth review of literature in skeletal system diseases. This has determined gaps in the research knowledge; how can the patient prognosis of skeletal implants be improved by novel design and manufacturing techniques? Can an implant/structure be created, which is more responsive or mechanically suitable? Multiple types of bone implants were explored, and in the area of lower limbs (e.g., hip, knee implants), a comprehensive volume of research has already been conducted. Further exploration of materials, biomaterials, and Functionally Graded Materials (FGMs) was undertaken. It was determined to focus on the mechanical requirements for skeletal implants, which thereafter led the research towards scapular supporting structures. In this area, rare recent studies have investigated the opportunities that 3D printing can offer, yet there were no data about the micro design of the material. This project future aim is to examine the benefits of designing material compositions and meso structures via 3D printing heterogeneous implants.

2 Background

2.1 Scapulectomy

2.1.1 Clinical problem

Scapulectomy and limb-salvage surgery are shown for moo and high-grade tumours of the scapula and soft-tissue sarcomas that auxiliary attack the bone. After adding up to or fractional scapulectomy, there are three choices of remaking: humeral suspension (flail bear), add up to endoprosthesis and massive bone allograft. These days prosthesis and allograft reproductions are the foremost utilised, and humeral suspension is saved as it were as a rescue method when no other surgery is conceivable. A few ponder clear separations and wound contaminations as the major visit complications of the scapular prosthesis account for 10-20%. As of late, within the endeavour to avoid these complications, a few creators have utilised homologous allografts to supplant bear support after scapulectomy for bone tumours, avoiding common complications of the scapular prosthesis [1].

Scapular remaking after tumour resection could be a secure strategy and can be performed with excellent functional, oncological and corrective outcomes but in reference centres and by expertise specialists. Hayashi et al.[2] showed three scapular reproductions taken after resections for scapular tumours (chondrosarcoma in all cases), and the distinctive reconstruction alternatives were analysed and portrayed. The ultimate message was to send these uncommon tumours to reference centres where a multidisciplinary group could treat these rare substances, and oncology specialists could arrange this complex surgery.

Before the arrival of chemotherapy, patients with bone tumours were mutilated. Nowadays, due to the technological advances of biomedical engineering and surgical techniques, non-amputating techniques have been proven safe and effective for bone tumours, with a percentage of success of more than 90%. After the extraction of a tumour, several reconstructive approaches are used, like biological, prosthetic and joined implants for bone repairment [3]–[5]. At present, a commonly used technique is the modular endoprostheses, which have evolved over the latest 40 years. This method shows satisfactory results concerning the recovery of the function and the rate of complications in severe incidences [4], [6]–[8]. Another widely used method is scapulectomy, which is the removal of the scapula when either a lower or a higher grade tumour exist, or other invadable to the bone soft-tissues sarcomas [9]. However, most reconstruction methods showed inadequate performance outcomes, and there is room for developing more efficient implants [10], which this project aims to fulfil.

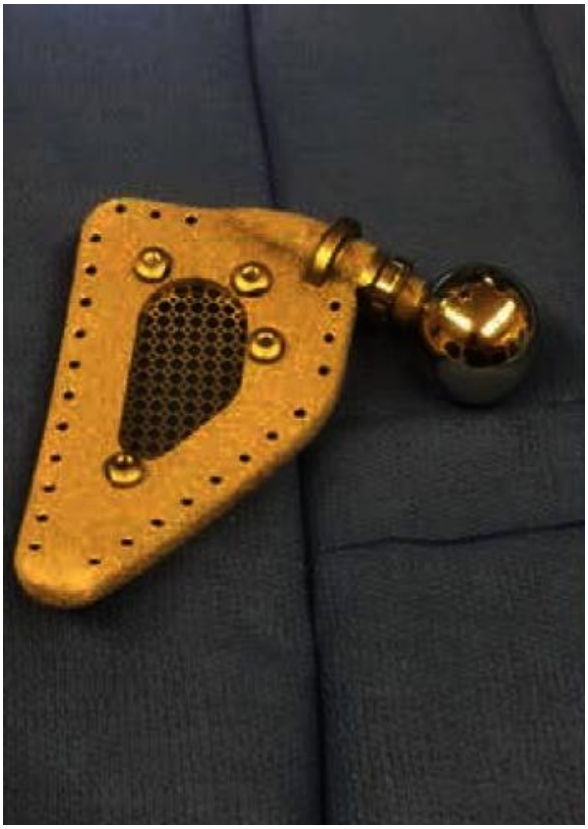

Figure 1. Scapular implant. Taken from[11]

After complete or partial scapulectomy, the three main options are the humeral suspension, the entire endoprosthesis, and the large bone allograft [9]. This research project is proposing a bone allograft that has advanced mechanical properties while being light weighted and design optimised. Nevertheless, conditions and sites with difficulty are emerging the need for anatomical patient-specific implants [3], [12]–[14].At the moment, a developing interest is being directed to additive manufacturing because it presents innovative solutions to such problems, enabling the customisation and personalisation of implants [13], [15]–[17]. Those types of implants are precisely tailored for bone injuries on various occasions, including oncologic and non, showing significant results [18]–[24]. The proposed implant follows patient's anatomy, while having advanced material properties by manipulating material meso structures, using lattice structures and TO techniques.

2.1.2 Scapular Implants

The design of scapular implants varies depending on patients' needs and design engineers' available technological equipment. Subtractive manufacturing methods, like milling or turning, could not enable patient-specific anatomical implants, and scapular bone cavities could not be manufactured because of this bone's specific details. An instance of an implant (Zimmer Biomet, Indiana, USA) for total scapular prosthesis is shown in Fig.1. Inevitably, the geometry of the actual scapular bone is not followed [11]. In contrast, Additive Manufacturing (AM) methods enable more freedom in implant's design and advanced designing capabilities.

Fan et al. [25] represented in a case series of patients with limb salvage surgery. In one of them, a 35-year-old woman with right scapular Ewing's sarcoma was diagnosed with a tumour that arose from the scapula that had spread into surrounding muscles, forming a long soft tissue mass. The patient's image data from MRI and CT were imported into CAD software to reconstruct a 3D tumour model (Fig.2A). Then, the other symmetric scapular bone data were introduced to create an anatomical patient-specific implant (Fig. 2B). Next, the scapular bone was removed, and the additive manufactured porous titanium implant was inserted following the bone's exact anatomy (Fig.2C, D).

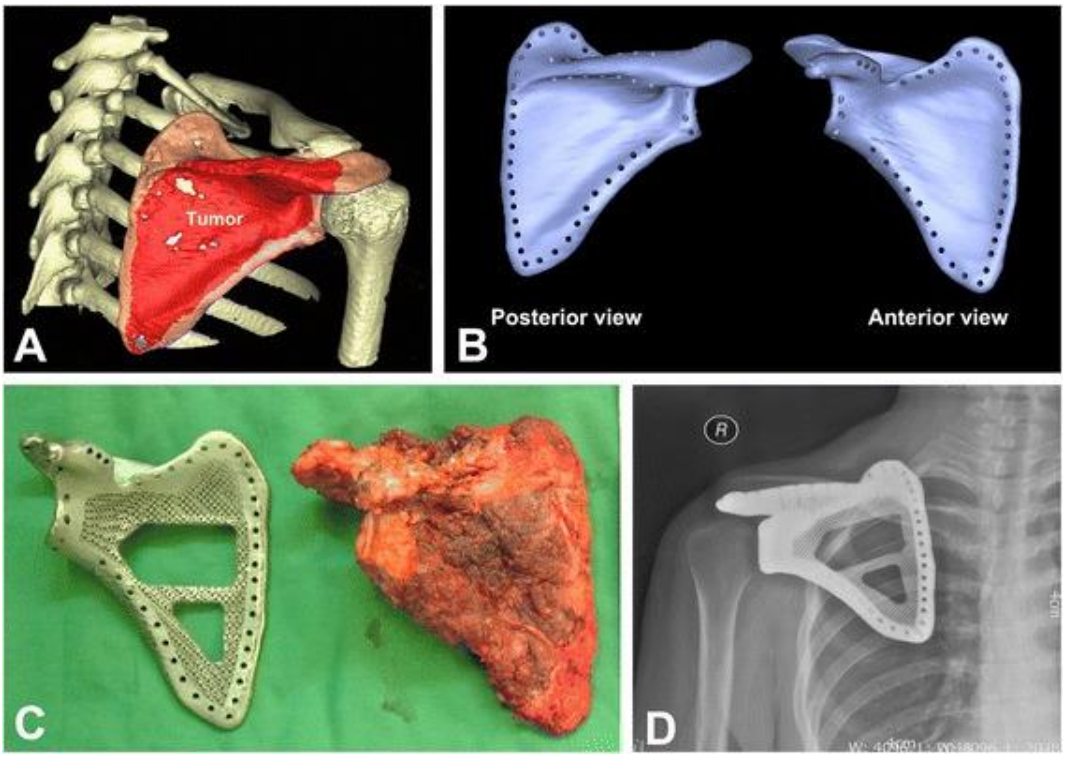

Figure 2. A) Recreated 3D scapular tumour representative. B) The virtual 3D replica of a scapular prosthesis. C) The dimensions of excised tumour and prosthesis were well fitted. D) X-ray demonstrated an appropriate shoulder representation 21 months after the operation. Taken from [25]

2.2 Additive Manufacturing (AM)

The AM or 3D printing process, is a manufacturing method that enables the of a 3D CAD model to be constructed as actual object [26]. The term AM covers a group of processes in which the material is deposited, solidified or joined layer by layer[27]. The entire procedure involves converting CAD files into Computer-Aided Manufacturing files (CAM) by exporting Standard Tessellation Language files (STL), as shown in the flow diagram of Fig.3. STL is a file format for stereolithography CAD software created by 3D systems [28]. Other than STL files, many other file formats for AM have recently been released. These include AMF and 3MF files. The STL file can be imported to a slicing program depending on the printer's compatibility. A G-code can then be exported from the slicing program to be used in the printer's interface. It can be transferred in text format either on a USB stick or memory card. Different materials can be used in different printing conditions and with different material properties. For this research, a metal 3D printer was intended to be operated. However, COVID-19 made it impossible to achieve this goal. It is essential to consider the most common barriers to additive manufacturing design, including education, cost, validation, and finishing [28], to create a realistic model.

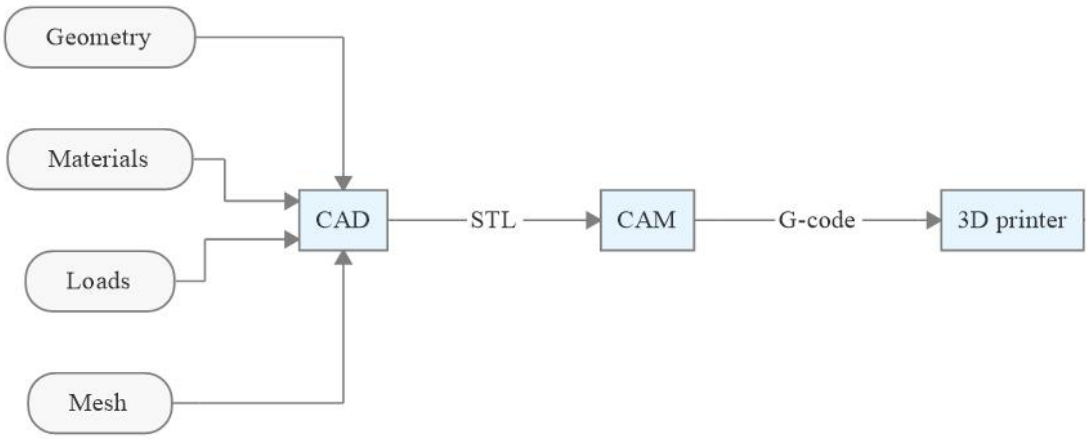

Figure 3.CAD to CAM translation flow chart

AM or 3D printing is one of the most novel technologies used in the biomedical field, with numerous unexplored possibilities. AM is an emerging technology used for bone reconstructions, complicated revision surgeries for challenging sites where modular prostheses are unavailable [29]. The chance of custom-made 3D-printed prostheses enhances their application in the surgical field despite the complication rate, obtaining much attention for potential advantages [30].

Three-dimensional (3D) printing innovation has gotten incredible consideration within the past decades in the academic community and industry since its focal points include customised manufacture, moo fabricating taken a toll, exceptional capability for complex geometry, and a brief creation period. 3D printing of metals with controllable structures speaks to a state-of-the-art innovation that empowers the advancement of metallic inserts for biomedical applications. This audit examines existing 3D printing methods and their applications in creating metallic medical implants and devices [31].

2.2.1.1 AMF file

AM file format (AMF) is a standard for representing objects for AM processes (ISO/ASTM 52915:2016) [32]. The official instance is an XML-based configuration created to define the shape and

configuration of any 3D model fabricated on any 3D printer via CAD software. Unlike its ancestor (STL format), AMF includes colouring, textiles, lattices, and constellations [33].

An AMF can interpret one object or various objects ordered in a constellation, where each object is defined as a collection of non-overlapping volumes, and each volume is represented by a triangular mesh that references various points. These points can be shared amongst volumes referring to the corresponding object. In an AMF file, the material and the colour of each volume, and the colour of every triangle in the mesh can also be defined. The AMF file is compressed utilising the zip compression format, but the '. amf' file extension is maintained, and a minimum AMF reader implementation can unzip an AMF file and import the geometrical information [34].

2.2.1.2 3MF file

The 3D Manufacturing Format (3MF) is an open-source file format standard formed and revealed by the 3MF Consortium [35].

The 3MF data format is XML-based and is created especially for AM. It involves information about colours, materials, and other details that the STL format cannot illustrate [36]. 3MF is not expected to contest the standard CAD space, characterised by neutral formats [37].

Corporations of CAD software such as Netfabb, Autodesk, Dassault Systems, and PTC belong to the 3MF Consortium. Different companies in the 3MF Consortium include Microsoft (for the operating system and 3D modelling support), SLM and HP, whilst Shapeways is also added to provide a better understanding of 3D printing knowledge. Other essential parties in the 3D printing and AM business, such as 3D Systems, Stratasys, Siemens PLM Software, and Materialise, have latterly joined the consortium [38]. 3MF Consortium has also publicised a C++ application of the 3MF file format to encourage its adoption.

Following is a record of various benefits of the 3MF configuration [39]:

i. Full-colour and surface mount in one file
ii. Support designs connected to part details
iii. Complete tray asset for straightforward machine preparation
iv. Viewing, printing, and thumbnails in Microsoft Windows
v. Functional storage of beam lattices
vi. Numerous material asset
vii. Developed to be used in industrial manufacturing
viii. Native integration with Paint 3D and Microsoft Office

2.2.1.3 DICOM file

A DICOM file is an image stored in the Digital Imaging and Communications in Medicine (DICOM) format. It includes an image from a medical scan, such as an ultrasound or MRI. DICOM files may also involve identification data for patients to connect the image to a particular person.

The standard of DICOM is generated by the National Electrical Manufacturers Association (NEMA) and the American College of Radiology (ACR).

It was difficult for anyone except the producers of magnetic resonance imaging machines or computed tomography to decode the images at the beginning of the 1980s. Radiologists and medicinal physicists needed to utilise the photos for the dose-planning concerning the radiation therapy. NEMA and ACR merged their workforces to create a standing organisation in 1983.

In 1985, their first model, the 'ACR/NEMA 300,' was published. It was titled "Digital Imaging and Communications". It was obvious that modifications were required shortly after the model's announcement. The text was unclear and contained internal inconsistencies.

The next version was released in 1988. Vendors more widely recognized this version. Picture transmission was defined as using a dedicated two-combined cable (EIA-485). Georgetown University hosted the first 'ACR/NEMA 2.0' interconnectivity technology, May 21-23, 1990. Six companies participated in the event: General Electric Medical Systems (Merge Technologies), Siemens Medical Systems (acquired by Kodak), 3M, and DeJarnette Research Systems. These same vendors exhibited industrial equipment supporting ACR/NEMA 2.0 at the Radiological Society of North America in 1990. The second version that needed to be rewritten was quickly recognized by many. Various modifications to ACR/NEMA 2.0 were made, such as Papyrus (Standard Product Interconnect) and SPI ("Standard Product Interconnect"), which were inspired by Philips medical systems.

In 1992, the US Army established the first large-scale deployments of the ACR/NEMA technology as part of the Medical Diagnostic Imaging Support (MDIS)[40]. Performance-based at Ft. Detrick in Maryland. Loral Aerospace and Siemens Medical Systems supervised a group of corporations that practised the primary US army Picture Archiving and Communications System (PACS). This system was used at all major Army and Air Force medical healing centres and many US military hospitals. Merge Technologies and DeJarnette Research Systems created the modality gateway interfaces from third-party imaging modalities to Siemens SPI interface. This agreement also provided systems for the Navy and Veterans Administration.

The third version was published in 1993. The model's name was changed to Digital Imaging and Communications in Medicine, abbreviated DICOM. The Conformance Statement was created, new service classes were created, network support was expanded, and new service classes were added. To detect DICOM from its antecedents, "DICOM 3.0" was initially assigned to the DICOM standard [41]. Since 1993, DICOM has been continuously updated and expanded to make modifications backwards compatible unless the original spec is incorrect or vague. The current standard is the only "version" of DICOM. The "3.0" version number has been removed. There are no "insignificant versions" to the bar, and there is no modern way to create a new, inconsistent understanding of this pattern. It is unnecessary to mention the date of publication of a unique format [42].This excludes situations requiring particular conformance conditions, depending on a resigned element that is not documented in the current standard.

Although the DICOM standard is widely accepted by medical imaging equipment manufacturers and healthcare IT organizations, it has some weaknesses. DICOM is a standard that addresses technological interoperability issues in medical imaging. It does not provide a framework or architecture to create a clinical workflow. Integrating the Healthcare Enterprise (IHE) is an action that overlays DICOM (and/or HL-7) and defines profiles that allow you to choose features from these standards in order to implement transactions for medical imaging interoperability use case scenarios.

Although always compatible with the Internet and based upon transport over TCP transport, there is an increasing demand to support port 80 HTTP transport in order to make it easier to use within the web browser. A family of DICOM RESTful services has been created to allow mobile devices to access DICOM objects and services via the web. These include WADO-RS and STOW-RS [43].

2.2.1.4 DICOM and AM

There are many steps in obtaining physical models of bones such as the cranium, pelvic, and scapular bone for various implants using patient specific CT scan data. These include identification of a person, obtaining CT data in DICOM format and converting DICOM data into 3D STL or CAD models. In addition, design and analysis of customised implants and the manufacturing of models and implants using AM [44].

To collect CT/MRI data from a patient. This is the first step towards creating patient-specific physical modelling. A patient is identified in collaboration with a doctor, a hospital, or another healthcare provider. A CT scan or MRI identifies the patient's defect site. CT/MRI data contains 2D images that generate a 3D model for the specific bone/tissue. A spiral scanning technique can be used to ensure that these images are accurate and precise. Complete volume scanning produces large numbers of slices and allows for the adjustment of the size of each slice according to the case. DICOM is used to store the CT and MRI data [45].

2.2.1.5 Conversion of DICOM files to STL standard

A CAD model of the tissue/bone is required for additive manufacturing. Only 2D images are included in DICOM data from CT/MRI machines and must be converted to CAD models before being input to an AM machine. There are many proprietary software packages (e.g. MIMICS, Materialise, Belgium; 3D Doctor, Able Software Corps, USA; Geomagic Freeform and 3D Systems, USA; Geomagic Freeform, 3D Systems, USA;) as well as open-source (e.g. DeVIDE, Visualization Group; InVesalius, Brazil, Osirix, Switzerland) available for this purpose. These packages enable us to visualise and create a 3DCAD model of 2D images using image manipulation and segmentation. The distinction between soft and hard tissues/bones during image manipulation is needed [44].

Segmentation is a way to achieve this. Segmentation refers to the process of separating structures. The model should include the unwanted adjacent structures. There are many image segmentation methods available, including region-based and edge-based and threshold and feature-based. Most software programs use the threshold method. This tool uses the threshold method to define a range of grey densities. It expresses pixels that correspond to the osseous tissues. It may seem like a simple task, but it is a vital aspect of the actual process. If the range is not appropriate, it can lead to thickening and/or thinning of the osseous structures of interest. These structures may be removed during the process and cause undesirable dimensional changes. In order to locate the correct region of interest, a surgeon and radiologist can be very helpful. They will need to separate bone from tissue, exclude anomalous structures, and remove noise. A 3D virtual model is created of the tissue desired after segmentation. The biomedical software saves the 3D model as an STL file [46].

2.2.1.6 STL models processing

STL converts the surface into small triangular features. The process of turning the 3D model into an angled model can be imperfect and may include errors such as flip normal or gaps between triangles. These errors can be fixed using software such as Magics RP (open-source software), Materialise Belgium, Mesh Lab (open-source software), or Mesh Lab (open-source software). The number of triangles in the faceted bodies can also be adjusted to increase or decrease the model's surface quality [44].

Once the STL files for the implant designs and parent bones have been created, they can be input to an AM machine. There are two ways to get the final ready-to-use implants made using additive manufacturing. One is direct manufacturing of readymade implants, and the other is rapid tooling. In the former case, AM machines must be capable of fabricating implants in biocompatible materials such as titanium alloy (Ti6Al4 V), stainless steel (316L), CrCoMo alloy PEEK (poly-ether-ether-ketone), calcium phosphate/sulphate. This is possible using AM processes such as EBM (electron beam melting), SLM (selective lasing melting), SLS [selective lasintering], LENS (laser engineered network shaping), FDM, fused deposition modelling), and 3D printers. This is a good option if a high-end AM machine is not available that can manufacture metallic implants. Even a low-end AM can be used to make a prototype of an implant in this instance. The prototype does not have to be made from a biocompatible material. The prototype can then be used to make a silicon or sandy mould that is used to cast biomaterials end-use implants. Sand moulds are used for casting metallic implants. However, silicon moulds can be used to make polymeric implants such as PMMA (polymethyl methacrylate) or an expendable wax pattern in the investment casting of the metallic implant [47].

2.2.1.7 Sterilisation and validation of implants

The implant must be tested for biological, chemical and mechanical properties after being manufactured. Before fitting into the patient's body, they must be sterilised to eliminate living organisms such as yeasts and bacteria. Implant failure or severe illness can result from the placement of an unsterile implant [48].

2.2.1.8 Evaluation of surface roughness

An implant-bone interface should have a certain degree of roughness. This encourages cell proliferation and enhances the implant's adhesion. A higher level of attachment to the implant is possible when the surface roughness value ranges between 1 and100 µm [49].

2.2.2 Metal 3D printing technology

In this section, a review on metal AM advances have been conducted to choose the appropriate metal 3D printing manufacturing technology for the proposed implant.

2.2.2.1 Selective laser sintering (SLS)/ melting (SLM)

Selective laser sintering [50] uses a powder-based technology. Lasers are used as energy sources to bond the powder layer by layer and solidify it. Powder must have refined grains and thermoplastic properties to allow it to flow, solidify and be viscous. The laser power determines the thickness of each layer. The laser moves along the cross-section of a piece according to its layer cross-section (Fig.4).

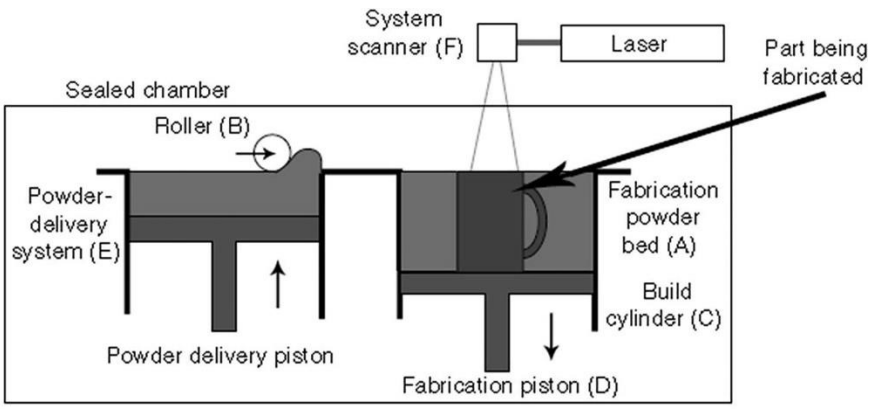

Figure 4. Laser sintering procedure. Taken from[51]

The main components of the system are a laser, scanner and roller. This SLS system spreads the powder from powder delivery to fabrication piston. The roller spreads powder onto the platform that is being manufactured [51]. Spreading powder requires a forward stroke with a roller. A similar roller is used to level powder on the fabrication platform by using a reverse stroke. A heating mechanism is operated to heat the powder below its melting temperature. This reduces porosity and thermal distortion, shrinkage, and the laser power requirement and increases the laser absorption. Most common heating mechanisms include resistive heaters as well as feed cartridges or infrared heaters.

After the powder is spread on the bed, the high-power laser beam scans the bed. The cross-section of the sliced part of the CAD model is used for the scanning [51]. The computer system controls the laser beam, and the scanning of that laser is integrated into it. This heats the powders cross-section of the sliced part sufficiently to melt the sintered and fine particles partially so that the current layer can stick to the previous layer. After the scanning of the current layer has been completed, the powder delivery piston and fabrication piston move up and down, and a new layer is deposited. The layer thickness of the powder bed determines the movement of the piston. The penetration depth of heat on the powder bed determines the power of the laser beam. Parts are made with a higher power laser beam. However, the layer thickness and thickness of the heat will affect the finish of the part. The process continues until all three-dimensional parts have been made. The powder is then removed with a pump and cleaned with brushes. The powder can then be recycled. It can take some time for the part to cool down before it is removed from the chamber. The overhanging part of SLS does not need any additional support. Instead, the unsintered loose powder acts as a support. This is an essential advantage of SLS. SLS parts can be used to create prototypes, models, moulds, and patterns for short-run production [52].

Materials:

i. Polystyrenes and Polyamides
ii. Thermoplastic Elastomers
iii. Bronze, Stainless Steel, Tool Steel and Zinc

Applications:

i. Prototypes: Investment Casting, Automotive Hardware, Wind Tunnel Models.
ii. End-Use parts: Electronics hardware, military, medical, aerospace, and other industries.
iii. Rapid production of tooling, fixtures, and jigs.

Advantages:

i. No additional support structure is necessary for the sintering powder.
ii. Parts exhibit high strength and stiffness.
iii. Complex Structures that include interior components are possible to be built without having to trap the material inside.

Parts can be printed with completely functional parts.

Disadvantages:

i. Porous and brittle
ii. Sensible to shrinkage, warping
iii. Creates excess waste
iv. Costly

2.2.2.2 Electron beam melting (EBM)

In the 1990s, the University of Sweden established the Electron beam melting process [53]. This is similar to the SLS method using powder technology. However, the electron beam of 4KW is employed to create a dense part. Porosity cannot be avoided due to the nature of laser sintering. When an electron travels at half the speed light strikes the powder surface, it causes the melting of the powder. This will produce kinetic energy. The electron beam is generally more efficient than a laser for conductive materials. Fig.5 illustrates a powder-based machine and how a part is constructed on an EBM. The part can be designed using a 3DCAD program or created using a CT scan from a patient. As explained in the previous section, the part is saved as an STL file and uploaded to the machine. Layer-by-layer, the part is made by melting metal powder using the EBM process. This results in a 3D part made of metal with a functional component that can be utilised immediately. Parts are manufactured in a vacuum. The chamber temperature is kept at around 1000 °C to enhance material properties and reduce internal stresses.

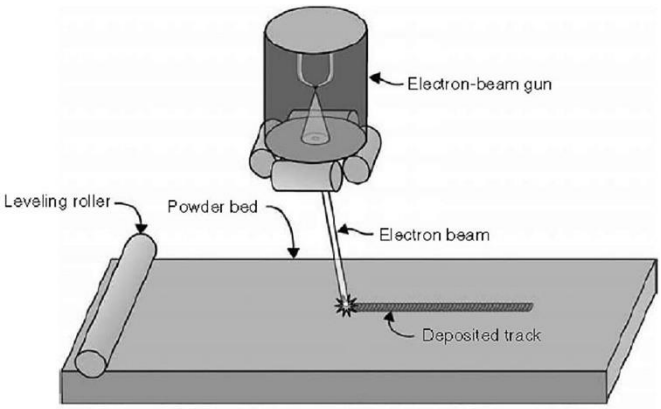

Figure 5. Electron beam melts powder utilising the speed of the electrons. Taken from [51]

The powder platform or powder bed is covered with a layer of powder metal. It is then placed in a vacuum chamber. Preheating a metal powder reduces the residual stress concentration and prevents distortion. The electron beam [54] gun can selectively sinter preheated metal powder by increasing or decreasing the beam power. These electrons are heated to 2500 °C and accelerated through anodes at half the speed of light. A magnetic lens brings the beam into focus, while another magnetic field regulates the beam's deflection. The beam of electrons focuses on

the powder bed. The kinetic energy is converted into heat energy to melt the metal powder. Controlling the number of electrons within the beam can control the power. To achieve a well-defined hardening, the cooling must be controlled. The parts will need to be final machined after fabrication, as with all other processes. Processing parts in a vacuum creates a calm environment which improves mental abilities. The powder bed platform is then lowered, and a new layer is added to the metal powder by using a roller mechanism. To level the powder bed, an identical roller is employed. The process continues until all three-dimensional parts have been completed. This process results in the creation of a dense part. The part can then be used to create models, moulds, tools, patterns, and prototypes.

Materials:

i. Chromium-Cobalt Alloys
ii. Titanium

Advantages:

i. Manufacturing speed. EBM allows the beam to be separated and heated in multiple places simultaneously. This significantly speeds up manufacturing speed. A laser must scan the surface.
ii. Preheating the powder prior to melting reduces deformations and helps reduce the need for reinforcements or supports during manufacturing.

Disadvantages:

i. Precision. The electron beam at the powder level is slightly wider than the laser beam, which reduces accuracy.

i. The maximum volume of components that can be produced. On the other hand, laser machines offer manufacturing volumes that are at least twice as large.

2.2.2.3 Direct metal deposition (DMD)/ Directed Energy Deposition (DED)

A group of AM processes that add material and input heat at the same time is Direct metal deposition (DMD) or DED [55]. A laser or electron beam can be used as the heat input, and for the material, feedstock wire or powder is applied [52]. A schematics of how the DED systems technologies work is shown in Fig.6 [56].

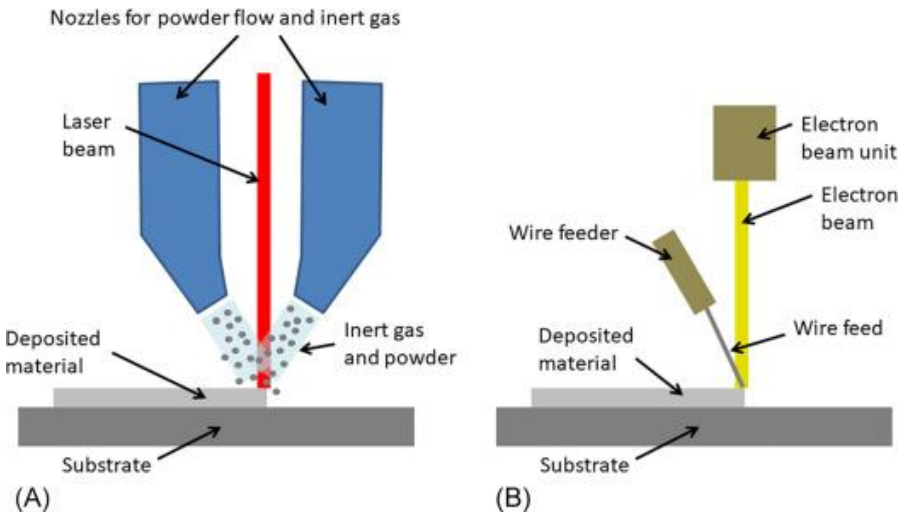

Figure 6. Illustration of two DED systems: (A) laser combined with powder feedstock, and (B) electron beam and wire feedstock. Taken from [57]

The basic system [58] works similarly to EMB and SLS. The melting of metal powder is a different process. In this case, the computer-controlled laser will be used. This will allow for direct metal manufacturing. The high-power laser is operated to melt powder metal and create dense metal structures. To validate mechanical and geometric integrity parameters, the part is constructed layer by layer using the software.

The entire system is enclosed in a transparent chamber filled with argon, so the oxygen level is below ten parts per million. The low oxygen level means that there is no impurity pickup during deposition. The laser beam is usually directed through the centre of the head and then focused on a small area by one or more lenses. Each object layer is constructed by the X-Y plane tables moving in a raster manner. The head then moves vertically up after completing one layer. The feeding system allows for small amounts of metal powder to flow very precisely. The metal powder is distributed and circulated around the head using gravity and inert pressurised carrier gases. An inert gas is employed whenever feeding is not necessary to protect the metal pool from oxygen. It provides better control over properties and better surface wetting to achieve layer-to-layer adhesion (Fig.7).

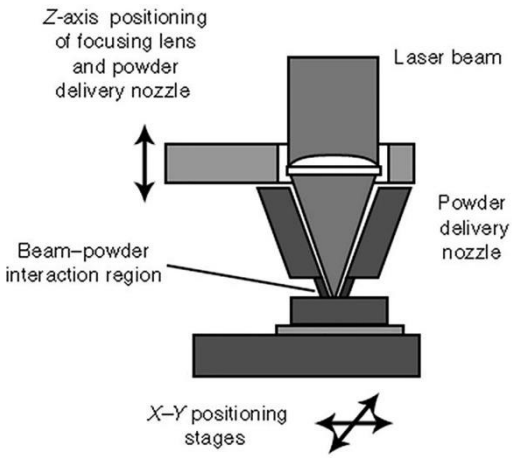

Figure 7. The schematics of the DMD process. Taken from[51]

Materials:

i. Inconel 625
ii. Stainless Steel applications
iii. Ti-6Al-4V
iv. Production of simple usable parts
v. Moulds
vi. Dies: Aluminium, Tool Steel

Advantages:

i. This method can create a part with excellent mechanical properties and a fully dense part at a very fast speed.

ii. The DMD process reduces the time to market, speed and cost of high-value components.

Disadvantages:

i. Surface finish, dimensional accuracy and microstructure control are all areas that need to be improved.

ii. Traditional DMD and RP processes utilise three-axis table technology. Support structures are often required for building overhanging parts.

2.2.3 Aspects influencing metal 3D printing performance.

i. Raw material's quality
ii. Environmental Controlled Machine Lab
iii. Ample Power Supply

Some defects may appear if these factors are not controlled.

2.2.3.1 Surface finish

Surface finish (Fig.8(a)) is the most crucial factor in any manufactured part. This usually requires machining after printing. Poor surface finish will result in a part that is less resistant to fatigue and will not meet the design specifications. The part must be post-processed to meet the design specifications. This increases the part economy's cost. The layer manufacturing part can look like steps on the part's surface, which results in poor surface quality. Finer powder particles are recommended to prevent this

kind of defect. A thicker layer can be printed with more delicate powder.

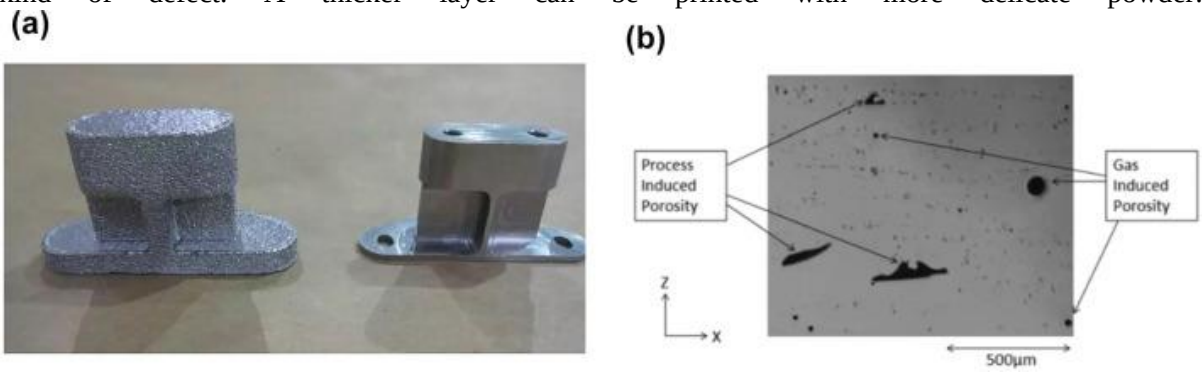

Figure 8. (a) Two Ti-6Al-4V brackets created of titanium alloy. (Image courtesy NASA). (b) Light-optical microscopy illustrates the comparison of the generated procedures. Taken from [59].

2.2.3.2 Porosity

Small cavities, known as porosity, are created when a part [60] is printed in 3D. This can occur due to the powder used or the 3D printing process. These microscopic pores cause a decrease in density, which can lead to fatigue and cracks. Powders that are too loosely packed or with a larger particle size than the thickness of the layer can increase porosity.

2.2.3.3 Density

Porosity is directly related to density. As illustrated in Fig.8 (b), the part's porosity [61] is inversely related to its density. The less dense a part, the more likely it will crack or fatigue under pressure. Critical applications require a density greater than 99 per cent.

2.2.3.4 Residual stress

The metal 3D printing process causes residual stress through contraction, expansion, cooling, heating, and cooling. If residual stress exceeds the substrate's tensile strength or printing material, then defects such as warpage or cracking can occur (Fig.9(a)).

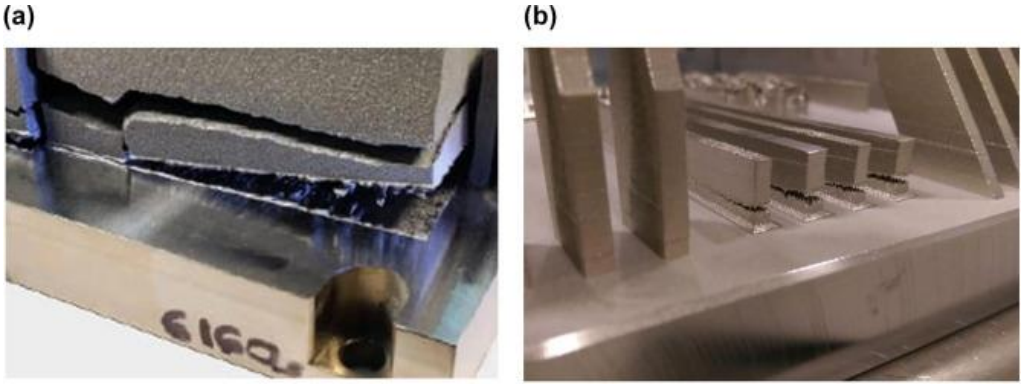

Figure 9. (a) Due to residual stress build-up, a titanium part is removed from the powder bed's build plate. (b) Cracks during the powder-bed process. Taken from [59].

2.2.3.5 Cracking

When melted metal solidifies cracking can occur, or when further heating is used to cause the pores to spring (Fig.9(b)). Stress can occur when the energy source used during solidification is too strong. Cracks between layers can also be caused by delamination. This can happen if the powder isn't melted enough.

2.2.3.6 Warpage

When the substrate's strength decreases, the temperature stress on the substrate causes a warp. The part will eventually warp and collide with each other when the powder is re-coated. The ideal number support structure should be located in a location where the warpage can be stopped (Fig.10).

Figure 10. Warpage (Image courtesy of the Centre for Additive Manufacturing and Logistics at North Carolina State University).Taken from [59].

2.2.3.7 Strength in Z-direction

Because of the continuous deposition of metal in X-axes, Y-axes, and Z-axes directions, the next layer is deposited after the first layer has been completed. Therefore, the vertically upward bond is weak. These layers have anisotropic bonds. These 3D printed parts have anisotropic properties, which means they can be measured in different directions (Fig.11).

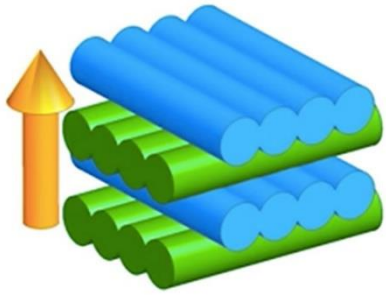

Figure 11. Z-strength can be measured by the strength and stability of the internal bond between layers of a 3D printer part. Taken from [59].

3D metal printer users such as industrial and commercial ones should understand the concerns about the overall part strength impact. They should also consider the end-use and function of their 3D metal printers. Every material should be rated in Z-direction. This section provided detailed information on the various methods for metal 3D printing as well as factors that affect strength in the Z direction, which is always an issue in metal 3D printers.

2.3 Optimisation Methods

Optimisation methods seek to improve the design of an object by adjusting the values of the design variables to achieve or even get as close as possible to the desired goal. These goals are usually related to the performance of the structure or the object's weight in general. Along with adjusting the values of the design variables, the restrictions are also checked as no one should be violated for this method to lead to a safe and achievable result [62].

In industry, a common way to improve their design construction, in general, is the method of trial and error guided by the experience of the engineer. Today, a significant boost in optimisations has been given by implementing systematic optimisation methods related to the FEA.

In an optimisation problem, the following elements must be defined: (i) design Space, usually defined as an area divided into finite elements, (ii) design variables, usually the density of finite elements located in the design space, (iii) objective function, e.g. mass minimisation, (iv) optimisation constraints, e.g. displacement restriction.

A variety of compositions have been developed from optimisation problems that vary based on the type of target and why they may differ depending on the purpose of the problem. The three main types of design optimisation problems are listed below, which are classified in order of increasing complexity and scope [63].

i. Size optimisation
ii. Shape optimisation
iii. Topology optimisation

In size optimisation, the values of selected dimensions that best achieve the design objectives are determined while meeting the existing constraints. For typical structure optimisation applications, the objectives could include minimising the maximum stress, strain energy, deflection or volume, or weight of an object. One or more of these quantities may also be formulated as constraints. For many mechanical parts, a small number of dimensions will be part of the optimisation problem. However, for cellular structures, such as grids, the number of design variables could be in the tens or hundreds of thousands [64].

Shape optimisation of an object or a given area is a generalisation of size optimisation. Typically, this method improves the shape of the curves or surfaces that delimit the area defined by the user. Thus, the control points of the respective curves or surfaces of the model can often be used as design variables. The above two optimisation methods are often combined to achieve structures with either a free-form shape or a standard one (e.g., a cylinder) with dimensions [65].

Finally, the TO determines the overall shape, layout of the elements, and connection to the design area. The main differences between TO and shape or size optimization are due to the different initial configurations and the choice of variables. These differences can lead to significant improvements in the structural performance of the model. The recent interest of the scientific community in TO as a design method for production with additive methods justifies a closer look at this technology [66].

For example, supposing that there is a design problem that requires structural optimisation, the size, shape, and topology of a product will be optimised separately or simultaneously. These concepts are essential to finding an optimal size, shape, and distribution during product development. As shown in Fig.12, size optimisation deals with optimising the size of an object (length, width, or depth). Instead, shape optimisation aims to find the optimal shape of a section or holes in the object. On the other hand, TO deals with optimising the entire geometry of the section, including size and shape [67].

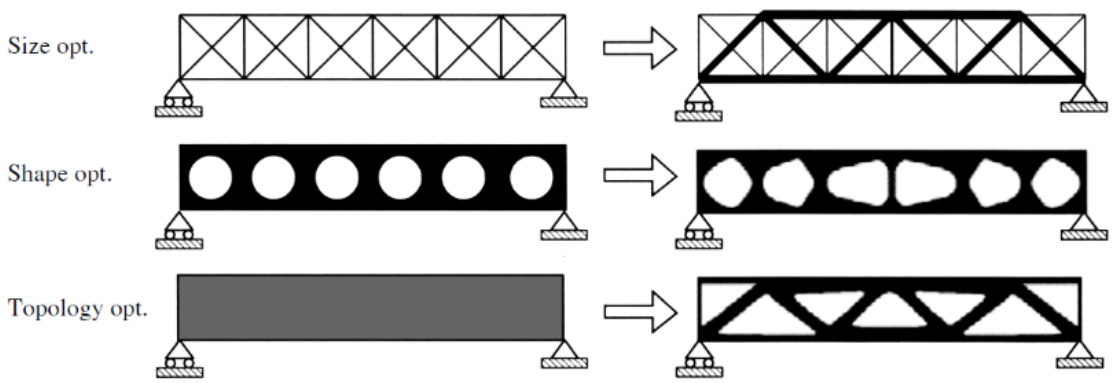

Figure 12. Comparative illustration of size, shape, and topology optimisation. Taken from [68]

An optimisation problem has the following general form:

$$min \quad f(x) = f(x_1, x_2, \ldots x_n) \qquad (1)$$

$$Subject \quad to: \quad g_j(x) \leqslant 0 \qquad j = 1 \ldots m \qquad (2)$$

$$x_{iL} \leqslant x_i \leqslant x_{Ui} \qquad i = 1 \ldots n \qquad (3)$$

Where f (x) is the objective function, $g_j(x)$ is the constraint function, x is the vector of the design variables.

The constraint is considered to be violated when g> 0.

Constraint functions are the model responses that result from FEA.

2.3.1 Advantages of Optimisation

Structural optimization, in general, has enormous potential benefits in the product development process. TO, in particular, has benefits in the design process like the creation of light structures and a ready-to-build plan, saving a considerable amount of material and processing energy, reducing the construction of natural prototypes and physical tests, while diminishing the market entry time [68].

2.3.2 Topology Optimisation (TO)

Reducing the mass and weight of the components in products can produce significant benefits such as improved efficiency and reduced material costs. By figuring out how to reduce mass without compromising structural integrity can be a real challenge. TO can help find the best lightweight shape for the wanted parts that will still meet the performance requirements. This project demonstrates how sim centre 3D with NX Nastran TO can be used to get the best shape for a new scapular implant design.

Optimisation methods focus on the topology of an object while determining the overall configuration of the elements in each design area. In general, they are structural optimisation methods, which implies the need for Finite Element Analysis (FEA) during each iteration during its implementation. A consequence of this is that TO has high computational demands. The factors that depend on the computational cost of this method will be examined in more detail.

TO is a mathematical approach for materials layout optimisation inside specific design space for particular boundary conditions (e.g. loads, constraints) for optimum performance [69]. TO differs from shape and size optimisation because the design can have any shape inside the design space [69]. For performance evaluation, the Finite Element Method (FEM) is used. The static analysis of a structure is possible using FEM, a broadly utilised engineering and mathematical modelling approach for solving differential equations. Therefore, it is also referred to as FEA [70]. In TO, the most utilised methods are mathematical programming gradient-based or non-gradient-based algorithms. Examples of those methods are the optimality criteria algorithm, moving asymptotes and the genetic algorithms [69].

2.3.2.1 TO Methods

Size and shape optimisation problems manage parameters related to the size and shape of the components of a structure, respectively. This means they can have a value between the limits set without changing the number of elements that make up the structure. If the optimal shape and size of an object are not known, TO should be utilised. The two main features of TO are that the elastic properties of

materials can vary along the design area (as a function of their density), and secondly, the material can be permanently removed from the design area [62].

Several TO methods can be grouped into two categories, optimality criteria methods and heuristic methods[71], [72]. Optimisation criterion methods are indirect optimisation methods. Their characteristic is that they meet a set of criteria related to the behaviour of the structure. They are often based on the Kuhn-Tucker optimisation condition [73], making these methods particularly rigorous. Their use mainly concerns problems with many design variables and few constraints.

The methods that belong to the category of criterion optimization topology are Homogenization, Solid Isotropic Material with Penalization (SIMP)[74], [75], Level Set Method[76] and Growth Method for Truss Structures [75].

Regarding heuristic methods, they can be based on intuition, observations of engineering processes or even observations of biological systems. These methods do not guarantee that they will always find the best solution. However, they do provide sustainable and practical solutions. Some of the heuristic optimization methods are the Fully Stressed Design (FSD) [76], Computer-Aided Optimization (CAO)[77] , Soft Kill Option (SKO), Evolutionary Structural Optimization (ESO) [78] , Bidirectional ESO (BESO) [79], Sequential Element Rejection and Admission (SERA) , Isolines/Isosurfaces Topology Design (ITD).

2.3.2.2 TO Categories

The solutions of TO should include results whose structures are almost fully charged or have constant deformation energy throughout the geometry where the loading conditions have been applied. Two approaches to topological problems have been developed. The first is based on the distribution of beams (truss-based), while the second approach concerns the formation of the density of an initial volume (volume-based). Below, a more detailed report is made for each one to understand their role and the need to differentiate them [80].

The truss-based network topology approach is based on structural elements related to a grid of beams between a set of nodes in a given set of volume. There are cases where this grid may represent a complete graph or be based on individual elements. In problems of this kind, TO firstly identifies which supports are necessary (struts), then determines their size (e.g., diameter) and then removes the beams that do not meet the respective specifications [81].

2.3.2.3 TO Problem Configuration

The application of TO is preceded by the formation of the problem, which requires close attention. The problem must be adequately defined so that its solution provides the best possible solution. Below are the steps to follow when designing such a problem [68].

1. Determining the purpose of the problem, i.e., what should be achieved with the optimisation and under what criteria
2. Collection of necessary data and information
3. Defining the design variables, identifying, and defining the design variables that describe the problem. This number directly affects the computational cost of the process.
4. Determination of the optimisation criterion must be clarified, i.e., the evaluation and termination of the optimisation process. This criterion is the objective function that must be maximised or minimised according to the requirements of the problem
5. Determining the limitations, at this stage, the limitations of the problem are identified.
   Generally, an optimisation problem is formed in the following mathematical way:

$$\text{Minimize:} \quad f(\boldsymbol{x})$$

$$\text{Subject to:} \quad g_i(\boldsymbol{x}) \leq 0, \; i = 1, m$$

$$h_j(\boldsymbol{x}) = 0, \; j = 1, p$$

$$x_k^l \leq x_k \leq x_k^u, \; k = 1, n$$

Where f(x) is the objective function that will be minimized while satisfying the constraints g(x) and h(x), inequality and equality, respectively, x represents a vector containing the design variables, the number of which is denoted by n. Finally, we observe the lower and upper limits for the design variable x_k.

2.3.3 Density Method

The method used in this project is called the Density Method [82]. In this method, the design variable is the density of each finite element in the design space, taking values from 0 to 1. 0 represents the absence of material and 1 represents the material presented in that element. Intermediate prices correspond to fantastic material. The material's robustness is considered to be linearly dependent on the density. This is something that applies to the materials. For example, steel has a higher density than aluminium, but at the same time, is a more robust material. Therefore, an intermediate density value can be considered to refer to a material with a lower density. Of course, where such cases exist, mostly in constructions with only one material, simply the presence or not of the material makes sense. For this reason, the density method follows techniques that punish intermediate densities for pushing into a design with areas of only the presence or absence of material without intermediate states.

2.4 NX Nastran

The NX Nastran module is used from the Siemens NX software for the TO of the scapular implant. This 3D design package contains, as mentioned in the previous section, various solutions. The one that combines TO and includes lattice structures is called ‘SOL 200 Topology Optimisation’.

In this section, the process of preparing and executing a topologically optimised solution will be studied. Stages of this process are the definition of the design area, the design objective, the introduction of constraints and design objectives.

NX Nastran TO can be helpful for the design a new object as it can provide an optimal design proposal. This proposal is generated by the software based on the finite element model simulation and the load cases through NX Nastran. In NX various solvents for TO are included. In earlier versions, the Tosca Topology Optimisation solver was adopted. In the NX 12, Siemens introduced TopOpt add-in command while updates were added later to the original version. Nowadays, in newer NX versions, Siemens has significantly upgraded the TO by introducing new commands and features. This way meets the requirements of both design engineers and Computer-Aided Engineering (CAE) analysts [83].

2.4.1 Topological Optimasation Workflow

The work in a typical TO analysis, from the initial design of a model to the production of its optimal geometry, will be present. Firstly, the static analysis of the model should be done, and then the TO will be applied. The following is the analysis of the topologically optimised geometry, which essentially verifies the previous analysis results. Finally, the formatted model is introduced into the software for

further detailed design ready for the manufacturing processes [84]. Briefly, the tasks required are the following:

A. Static analysis

i) Create or import model geometry into software
ii) Discretisation of geometry
iii) Determination of material properties, loads and limit conditions

B. Topology optimisation analysis

i) Design objective setting
ii) Define design area and frozen areas (if any)
iii) Define optimisation constraints
iv) Definition of manufacturing constraints (if any)
v) Defining the form of presentation of the results
vi) Export the optimal geometry to an STL file

C. Confirmation analysis

i) Import the STL file into the modelling software, edit the model and insert lattice structures in the appropriate design area
ii) Repetition of static analysis to draw conclusions

2.4.2 Solution creation

Firstly, the model is designed and optimised. The model can be a simple design, a more complex one, or even an assembly of a mechanism. In addition, it may consist of solid sections, surface sections or a combination thereof.

The corresponding simulation files (Simulation - sim file) and finite elements (finite element method - fem file) must be created to start a simulation. The existence of two separate files is the possibility of multiple simulations based on the same fem file. In the NX environment, select the Application tab and then Pre / Post.

Then, the New FEM and Simulation command from the home tab is selected to create the desired files and proceed to the model simulation.

The following two windows that will appear by selecting the New FEM and Simulation command describe some simulation features automatically generated by the software. For renaming should be selected File → Utilities → Customer Defaults. Then, should be chosen, Simulation → Pre / Post → General → FE Model and Simulation Create.

In the same window, with indication 2, an idealised object can be created. This object is a PRT file containing a copy of the base model, in which geometry can be changed without affecting the original part [85]. So, in essence, many parts can be created that link to the original model, many FEM files that link to each idealised part, and multiple simulations that link to one FEM file. This function is intended to minimise the work required for performing different analyses on the same object.

When FEM and SIM files are created, the software environment is adapted to help the user. More specifically, the tabs at the top contain commands that lead to the distinction of the model, called meshing. Also, during the process, the software reminds the user to assign the appropriate material to the model. Commands for material assignment also exist on the home tab, and they can be selected at

any time point of the process. Another category of commands involves the connection of parts and their cellular structure. Often, the geometry of an object is necessary to be divided into individual sections for easier discernment and to apply loads or constraints to a specific part of the model and not to an entire surface. However, the model's parts should be connected because the object must have a single structure to study its behaviour during the simulation.

2.5 Convergent Modelling

Convergent Modelling ™ is a technology provided only by the CAD software NX (Siemens PLM, Texas, United States), which combines data with different capabilities, like Facet and B-Rep data [28]. Depending on the application, those geometric characteristics formats vary, resulting in one being more suitable than the other. Facet data are primarily used in gaming, animation, and digital mock-up because they are characterised by are triangular meshes that are more likely to produce more extensive data sets. In contrast, B-Rep data are primarily utilised in engineering 3D modelling because they can render more realistic solid volumes while using smaller data sets. Design engineers in areas like 3D scanning, TO, and AM usually generate many facet data that they want to use in 3D modelling systems only designed for B-Rep Data. Thus, convergent modelling technology enables data from both sources in one modelling environment to reduce errors, complexity, and conversion between different formats [28].

2.6 Lattice structures

In recent years several new materials have been developed with improved properties, the structure of which consists of a set of solid beams. These are designed to meet a variety of needs, such as weight reduction, heat transfer and thermal insulation [86], [87].Materials with a special mesh structure can be produced easily with AM methods. In general, AM involves processes that characterized by the layer-by-layer placement of the material and manufacturing of the object directly from the 3D model [88]. Structures designed for production through AM, referred to as Lattice structures, i.e., lattice or otherwise cellular structures.

AM enables the production of complex geometries that used to be difficult or impossible to be manufactured. Therefore, in parallel with the evolution of AM technologies, various strategies are also being developed for the cost-effective manufacturing of high-quality objects. The main advantage is that objects with specific stiffness and strength can be implemented, while at the same time, financial management of materials is improved. These are possible when combining AM techniques and TO. Nowadays, most CAD software packages enable the user to use TO and lattice structures. NX includes those features and their combination to help find the best solution for each design problem.

A lattice structure is a thin, rod-shaped design. Moreover, it can be used in AM to create light sections while retaining the characteristics of the structural ones, such as durability and integrity. When creating or processing a topologically optimised solution, one of the available lattice structures in the software can be selected. The optimum structure depends principally on the manufacturing requirements of the object [87]. Examples of different shape design for lattice structures are depicted on Fig.13 with various mechanical properties.

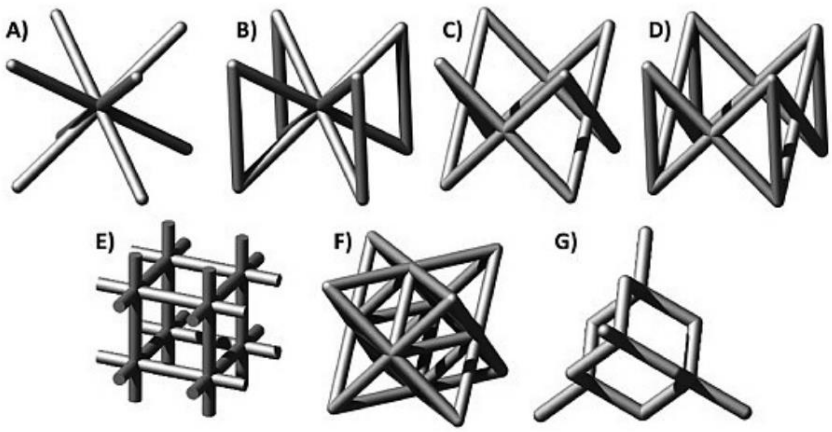

Figure 13. Strut-based lattices: BCC (A), BCCZ (B), FCC (C), FCCZ (D), cubic (F), Octet-truss (G), and diamond (H). Taken from [87]

3 Methodology

3.1 CAD Geometry

This project aims at the TO of a scapular implant and the subsequent lattice structures application. The implant design was performed using the Siemens NX Series 1899 software. Fig.14-18 show the initial model to which will be implemented methods as mentioned earlier. The model was downloaded from an internet website source called 'Cults', with free available STL file examples [89]. This STL file contains the anatomy of an actual scapular bone, imported from a Digital Imaging and Communications in Medicine (DICOM) file [42] and converted to STL previously. The procedure for importing this STL file to NX 1980 Learning Edition (Siemens PLM, Texas, United States) was: File → Import → STL, then in the STL file's input window, the model type was selected to be Convergent, and the unit of measurement was millimetres (mm). The model consisted of surfaces that were connected. Some parts of the bone-implant were intact because they will be in touch with the humerus, the key, the branchial muscles, and other soft tissues. In parallel, the mass will be reduced in other parts of the implant using the TO algorithm. In this project case, the STL file was used directly in the software, whereas the methodology for anatomical accurate patient-specific implants includes utilising a DICOM file, which consists of the upper body part bones, including both shoulders. Both shoulders are required because the healthy shoulder is mirrored to the other side, representing the exact geometry of the bone. The methodology of designing a personalised implant through symmetry has been widely used, mainly for cranial implants [90].

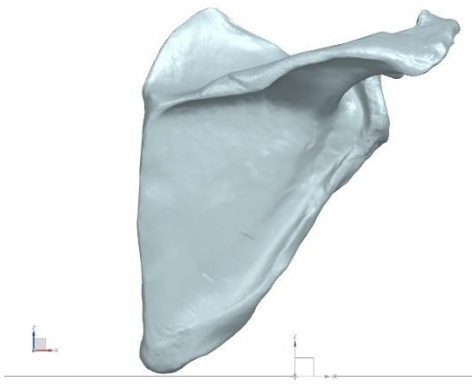

Figure 14. Model front view

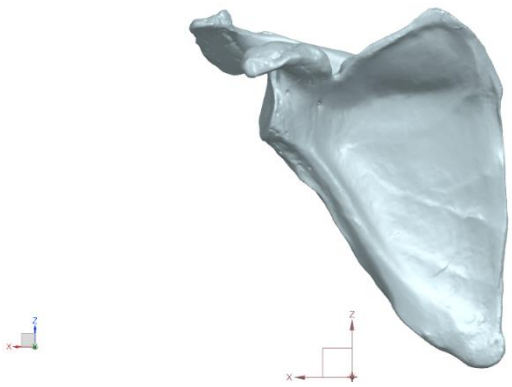

Figure 15. Model back view

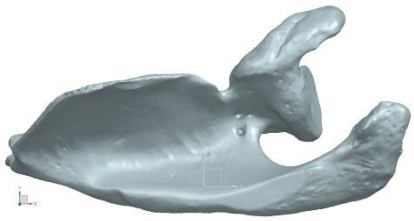

Figure 16.Model top view

Figure 17.Model right side view

Figure 18.Model left side view

Firstly, in the convergent modelling environment, it was allowed to sketch curves, so studio splines were created to split the model into different parts, which was helpful for the next steps. The next step was the command 'divide face', so the sketched spline curve was projected to the mode, and the model was divided into two different solid bodies, where Boolean operations could be applied in each of them.

The convergent modelling environment enabled direct working with the convergent body. Whenever the selection was changed to solid body, different areas were noticed. Then, the model was united in one solid body by using the command 'unite'.

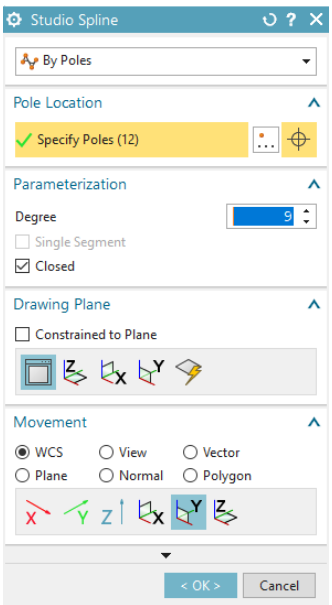

Figure 19. Studio spline

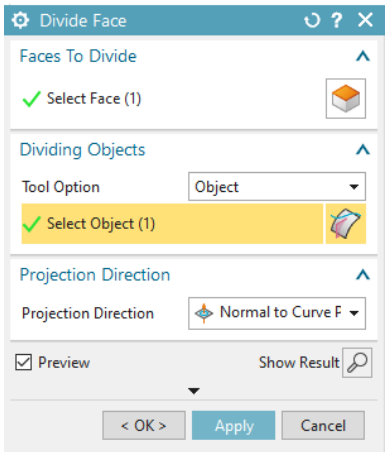

Figure 20.Divide face

3.2 Topological Optimisation Methodology

Through the NX Nastran solver, a new study was defined to perform the TO. In the first stage, the type of structure (lattice structure) and the operating conditions were determined. After the modification of the model, the simulation and solution had to be created. Firstly, the material Ti–6Al–4V was selected, and the model was distinguished by the FEM. Later, the loads were applied to the points that the bone receives stress, and the model's static study's boundary conditions were determined. Subsequently, the design goal was assigned, which is the reduction of mass, because, in this way, tissues can regenerate,

and eventually, the optimisation areas, but also those that will remain the same, called 'frozen areas', were set too. At the same time, a manufacturing constraint for additive manufacturing was placed, and in the later step, the model setup was conducted, and it was solved. Afterwards, the results were displayed, where material distribution was visible. Then, a gradual change in the thickness and density of the lattice structure could be tested to determine whether it is possible to apply functionally graded materials (FGMs) which exhibit increased mechanical properties [91].

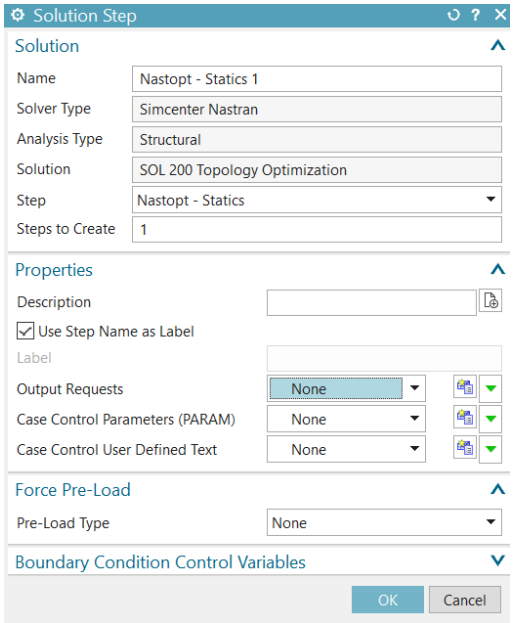

Figure 21. SOL 200 Topology Optimisation Solver

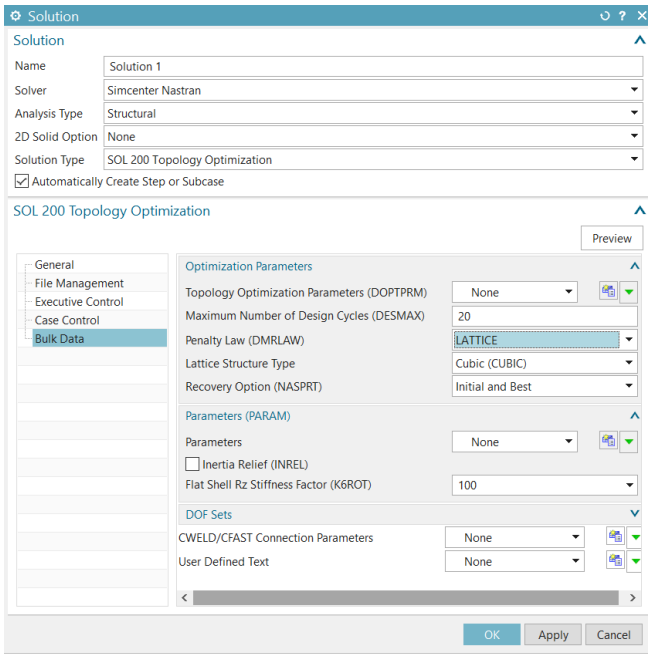

Figure 22. Results bulk data

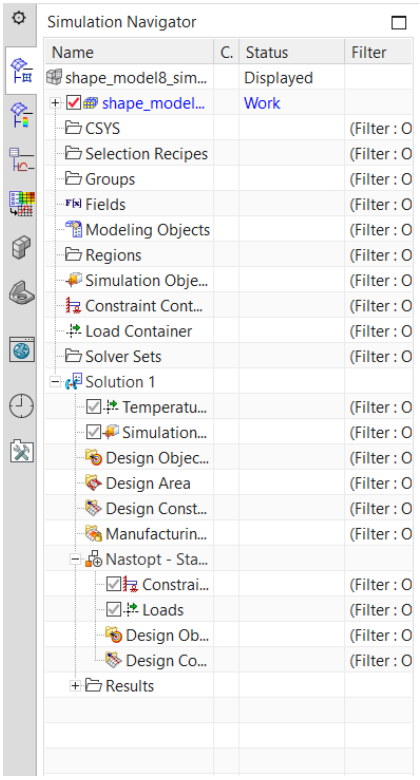

Figure 23. Simulation navigator with active meshing

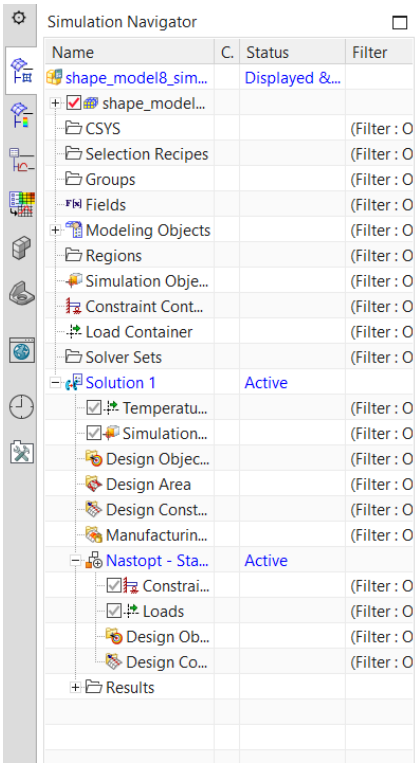

Figure 24. Simulation navigator with active solution

3.2.1 Materials

Next, the properties of the material to be used were defined and after a deep literature search the appropriate material was defined. Titanium Ti-6Al-4V (UNS designation R56400) [92] is applied in various bone grafts and shows significant results [15], [16], [18], [19], [24], [25], [92]–[95]. More specifically, the material, also called TC4, Ti64, or ASTM Grade 5, is an alpha-beta titanium alloy with extraordinary strength and superior corrosion resistance. This is a very popular titanium alloy, primarily utilised in various applications, such as the aerospace and the biomedical industry [93].

The commands required for this process are following, included in the simulation environment:

i. In the Home → Properties tab, select Physical Properties
ii. Physical Properties → Create → Physical Properties table → Properties → Material → Choose material→ Ti-6Al-4V

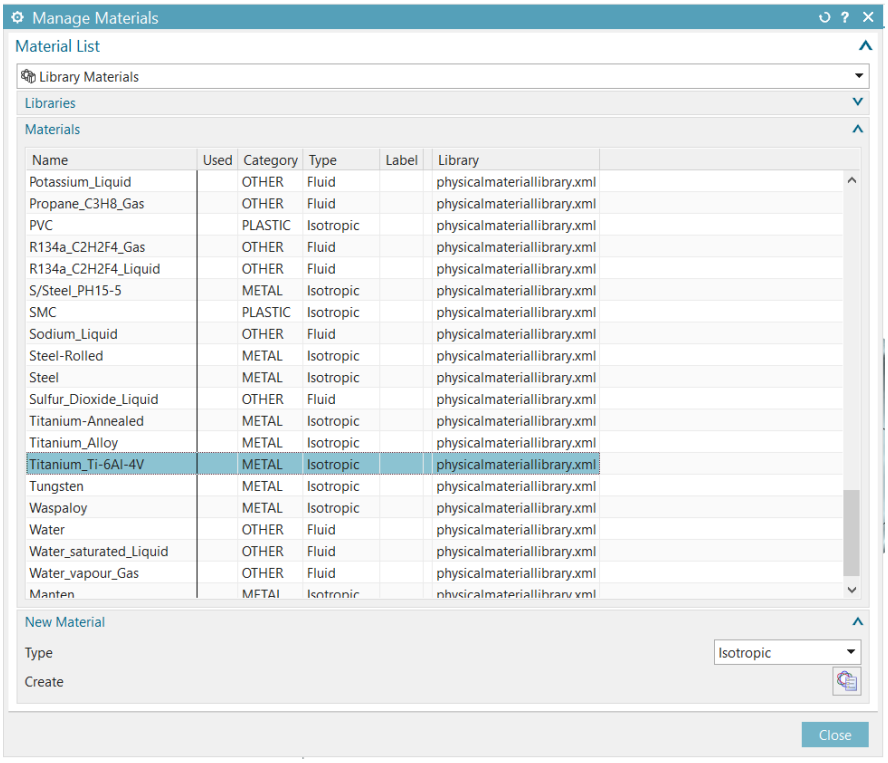

Figure 25. Manage materials section

3.2.2 Mesh

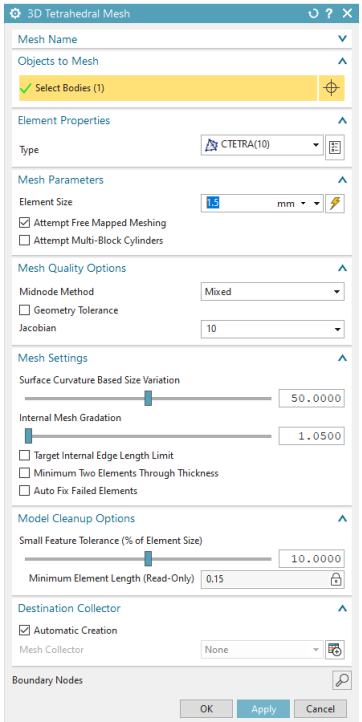

Figure 26. 3D Tetrahedral Mesh Creation

TO is a finite element-based approach, and the first step is the creation of the mesh for the entire design space where the part can live. So, the final model can fit anywhere within this mesh. So, the discretisation process is the next step to be done. The window for 3D tetrahedral mesh prompts the user to select the area they want to distinguish, and to choose the type and size of elements they want. This process will be repeated until all the geometry of the model is discernible. The 3D mesh, shown in Fig.26-32 consisted of 178108 elements.

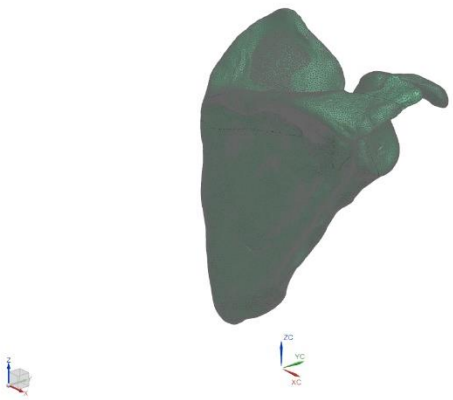

Figure 27. Mesh trimetric view view

Figure 28. Mesh front view

Figure 29. Mesh right side

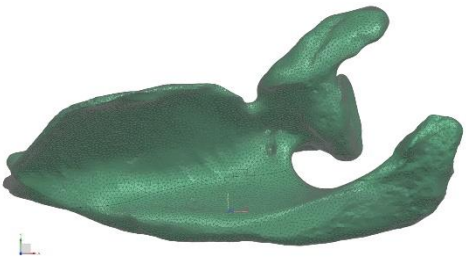

Figure 30. Mesh top view

Figure 31. Mesh left side view

Figure 32.Mesh back view

Then the activate simulation command was selected.

3.2.3 Design Area

After, the design space was determined, and some regions were kept from the optimisation run. The design area may refer to parts of the model which will be optimised (optimisation area) and in parts which will remain as they are (frozen area). It is helpful to specify only the data which will be optimised or just the frozen elements of the model so that the problem is not becoming more computationally expensive and to achieve more quickly converge to the optimal solution. In this project, it was chosen only to define the optimisation area as shown in Fig.33,34.

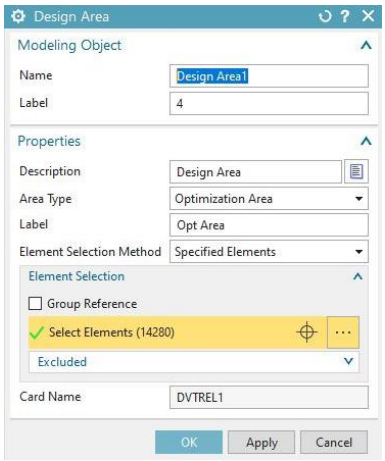

Figure 33. Optimisation area's elements assignment

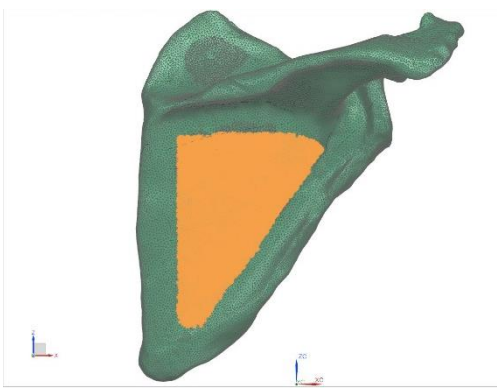

Figure 34.Elements of optimisation area in subscapular fossa cavity

3.2.4 Design Constraint-Global

Not needed areas exist in the space where there is no muscle attachment in the actual scapula. For this scapular implant, the aim is to minimise the total model weight, with an upper mass limit of 3.8 kg which is the upper limit of a human masculine scapula [96] (Fig. 35).

The design constraint must then be defined for optimisation analysis. In our case, as a parameter describing the constraint, it is the total model weight. Therefore, before each design circle the desired weight should be determined and the upper and lower limit of the restriction. In this project case the

lower limit is 0 kg and the upper is the 3.8 kg because the aim for the scapular implant is to weight less than the actual bone.

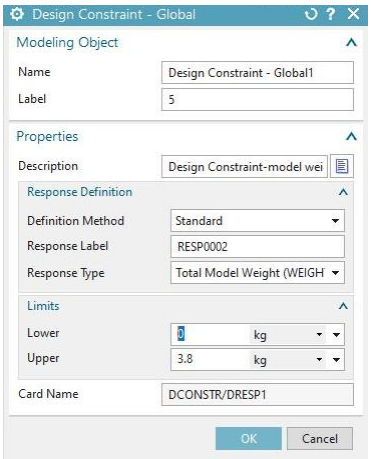

Figure 35. Design Constraint Assignment

3.2.5 Manufacturing Constraint

Then, a manufacturing constraint was set. Since it would be an additive manufacturing part, the maximum overhanging angle was assigned, which means the optimisation process will not create any over hanged angles that will make it impossible for the part to be 3D printed. The general rule for 3D printing overhanging angles is θ=45 degrees, but that can vary depending on the available technological equipment (Fig.36). Also, the layer height was assigned as 0.8 mm, because this is the minimum wire feedstock for the 'Meltio M450' metal 3D printer [97]. However, this parameter should be revised when the actual part is manufactured, depending on the printer's nozzle diameter and therefore the minimum layer height, generally assign as a minimum of 0.1mm [98].

In this step, the point for the 3D printing base plate was asked, and the base plate 'normal' vector, as shown in Fig. 37,38. The point for the base plate was chosen to reduce the overhanging geometry angles, and the 'normal' vector, usually assigned as z vector in 3D printing machines, was selected. In this case, this is the vector x because of the way the model was initially inserted in the software.

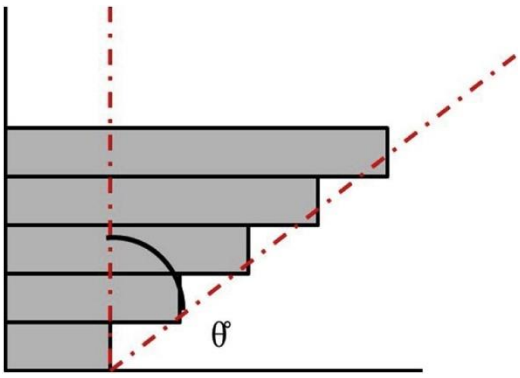

Figure 36.Material overhang associated with building on an angle θ. Taken from [99]

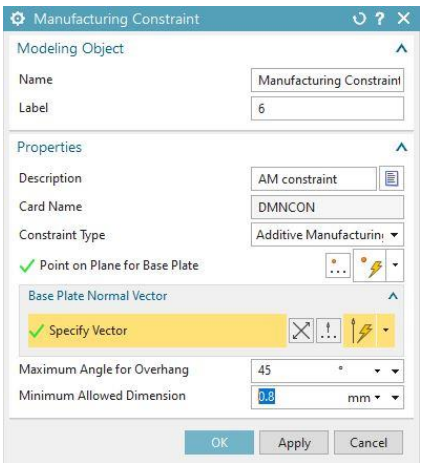

Figure 37. AM constraint

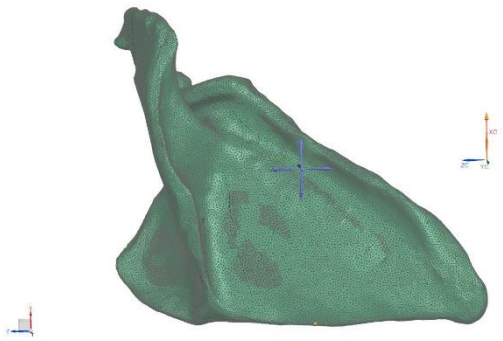

Figure 38. Point for base plate and base plate 'normal' vector

3.2.6 Boundary conditions

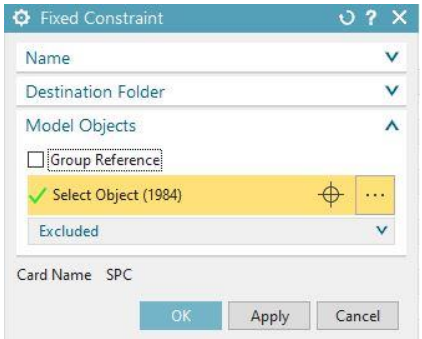

Figure 39. Fixed constraint assignment

For static analysis of the model, fixed constraints are added. The procedure for this command was the New Constraint→ Fixed Constraint. Fixed element nodes' Degrees of Freedom (DOFs) were equal to zero, meaning that these elements were constrained in directions x, y, z and could not rotate in any direction (Fig.39,40).

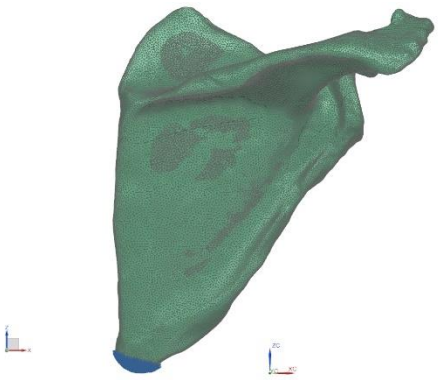

Figure 40. Fixed elements for static study

3.2.7 Loads

This step of the simulation process is complex because for the actual application of muscular loads. There are the following eleven muscles originated from the scapula: deltoid, supraspinatus, infraspinatus, triceps brachii (long head), teres minor, teres major, latissimus dorsi, coracobrachialis, biceps brachii, subscapularis and omohyoid muscles. Another six muscles insert on the scapula which are trapezius, levator scapulae, rhomboid major, rhomboid minor, serratus anterior and pectoralis minor muscles [100].

The simulation of the actual muscular loads could not be conducted because it was very computationally expensive, and server resources were not available for this research. Instead, a more simplified model of the pressure load was conducted, which approximates the scapular loading conditions found in the

literature. The surfaces that the pressure load was applied are all the external areas of the scapula except infraspinous and subscapular fossa, as shown in Fig.41. The data for the loads acting on the scapular bone in the literature were few. An interesting study conducted by Quental et al. [9] in subject-specific bone remodelling of the scapula included whole muscles and joint loads for six different scenarios of arm elevation degrees. However, it was so complex for these data to be inserted in the NX Nastran solver.

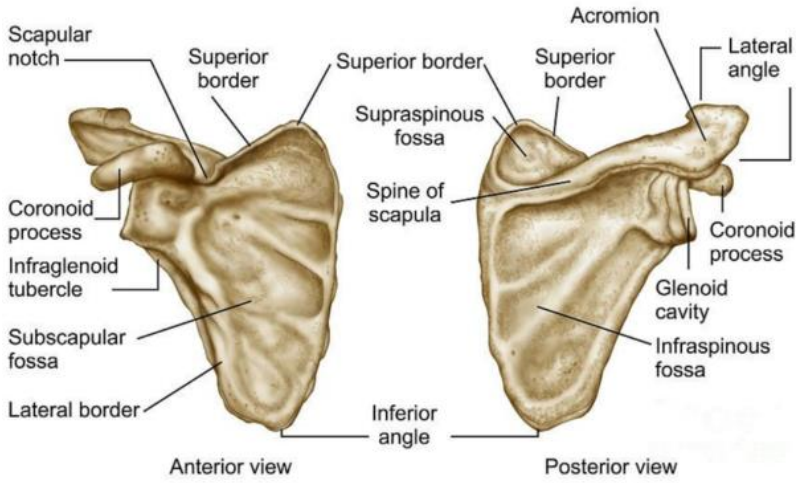

Figure 41. Scapular cavities. Taken from [101]

Instead, an average approximation of those loads was used. In another review article by Hart et al. [102] were interestingly analysed the forces that the bones undergo (bending, torsion, tension and compression) while showing the elastic and plastic deformation. This project imported data from average anisotropic values of ultimate strength (compression, tension, shear), elastic modulus and Poisson's ratio in cortical bones. As a result, the maximum values for the pressure load are the maximum longitudinal compression in cortical bones, which equals 193 MPa [102]. Maximum values were utilised for safety purposes.

For the application of the desired pressure load the commands are the following: Load Type → Pressure, select object: selection of the model's elements in the area pressure is applied.

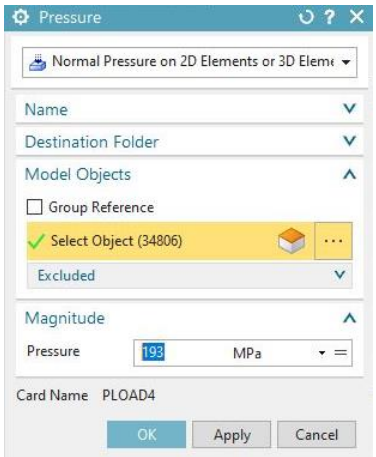

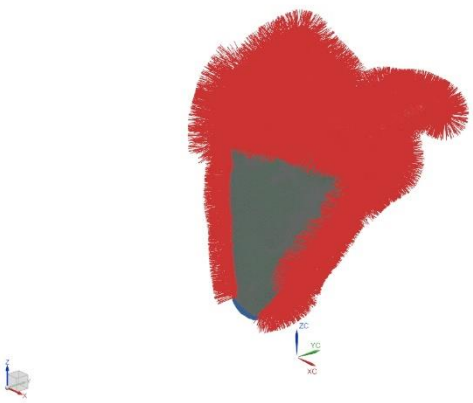

Figure 42. Pressure load assignment

Figure 43. Pressure loads graphical representation

NX Nastran TO allows the analysts to dig deeper than what can be done with the designer level TO tool. For example, TO in NX Nastran can support multiple solutions based on the same model to study

the effects of different load cases and analysis types. After defining the max number of iterations, 20 design cycles, in this case, the model was solved.

3.2.8 Solve

The purpose of applying TO with lattice structures is to develop a new, improved design with minimised flexibility and reduced weight. The TO method initially sets in all the elements of the model density equal to one. In the solving process, the density of the data is changed and inserted where necessary lattice structures are defined. The final optimal model set resulting from this analysis is usually a mixture of solids and lattice structures. The software determines the quantity and quality of lattice structures. Data density values indicate the type of lattice structures and the lower limits of solid and lattice areas. The file generated after TO and contained this information is a spreadsheet with the CSV format. NX does not have the capability of importing this file to present the new design graphically. There are other suitable software packages for this process. Then the model was solved.

4 Results and Discussion

4.1 Results

After solving the model, the results files were displayed as follows:

Solution Model Setup Check Error Summary
Solver is Simcenter Nastran
Environment: Simcenter Nastran – Structural
Solution is SOL 200 Topology Optimization
Boundary Condition Geometry Associativity Check Summary
No Boundary Condition Geometry Associativity Issues
Mesh-Based Errors Summary
Total: 0 errors and 0 warnings
Material-Based Errors Summary
Total: 0 errors and 0 warnings
Solution-Based Errors Summary
Total: 0 errors and 0 warnings
Load/BC-Based Errors Summary
Total: 0 errors and 0 warnings
Nastran Model Setup Check completed
Summary of Bulk Data cards written
| NAME | NUMBER |
| CTETRA | 178108 |
| DCONSTR | 2 |
| DMNCON | 1 |
| DMRLAW | 1 |
| DOPTPRM | 1 |
| DRESP1 | 4 |
| DVTREL1 | 1 |
| GRID | 294698 |
| GROUP | 1 |
| LOAD | 1 |
| MAT1 | 1 |
| PARAM | 7 |
| PLOAD4 | 48248 |
| PSOLID | 1 |

| SPC | 1984 |
Nastran Deck Successfully Written

Following the previous analysis, all the results were mounted in the Post Processing Navigator. The density plot was utilised to view TO results. The results of static analysis are consisted of design cycles. The convergence design cycle is a repetition of the algorithm in which its optimal design was created object. The solver converged the conceptual shape based on the loading conditions. All the iterations were also visible in the animation. The way the part took shape was also evident. The density of the material per element of the model was represented graphically through the Load case Independent Results →Normalized Mass Density - Elemental. Design circle 0 concerns the original geometry of the model, so there are all of its elements and geometry so that they have a density equal to the unit. In Fig.44,45, the density distribution for Ti-6Al-4V material is observed throughout the subscapular fossa, which is one of the main scapular cavities. Blue symbolizes the absence of material, while as much as the colour is approaching red, the density increases based on the scale found on the left. Next, the shape could be exported as a facet body to turn this concept into a usable part. For this purpose, the desired density level was selected, 0.5 in this case, and then exported.

In addition to the distribution of the density of each design cycle, the structure of the elements can be graphically examined. More specifically, the NX software enables the user to adjust (within the permitted limits) the solid and lattice structures areas. First, in Fig.45, the density separation for each structure (solid and lattice) is shown. Each change in the density of the material resulted in the change of its shape. Colours are adjusted to green when the density is assigned to the field of solid structure and orange when it belongs to the lattice structure.

Figure 44. Subscapular fossa scapular cavity. Taken from[103]

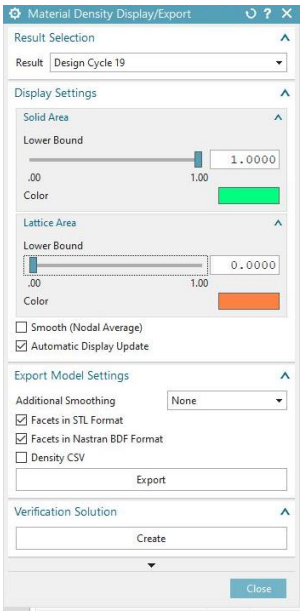

Figure 45.Material density results navigator

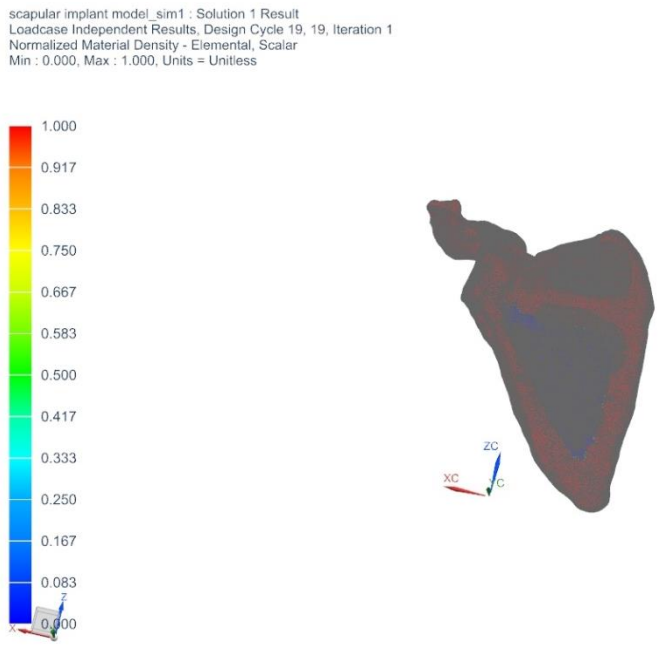

Figure 46. Normalised material density

So far, implant geometry was introduced in the NX software, and all problem parameters have been defined. Emphasis is given to the lattice structure type but also on the design constraint concerning the weight. Also, the model's weight could be reduced by up to 50% concerning the original.

Table 1. Objective function values

Cycle	**Design Objective Value**		**Most critical constraint Norm. Value**			
INITIAL	3.48E-01	-4.76E-01	Resp. Value	Bound Type	Bound Value	Resp. Type
1	3.33E-01	-4.77E-01	3.48E-01	<=	3.80E+00	WEIGHT
2	3.33E-01	-4.77E-01	3.33E-01	<=	3.80E+00	WEIGHT
3	3.33E-01	-4.77E-01	3.33E-01	<=	3.80E+00	WEIGHT
4	3.33E-01	-4.77E-01	3.33E-01	<=	3.80E+00	WEIGHT
5	3.33E-01	-4.77E-01	3.33E-01	<=	3.80E+00	WEIGHT
6	3.33E-01	-4.77E-01	3.33E-01	<=	3.80E+00	WEIGHT
7	3.33E-01	-4.77E-01	3.33E-01	<=	3.80E+00	WEIGHT
8	3.33E-01	-4.77E-01	3.33E-01	<=	3.80E+00	WEIGHT
9	3.33E-01	-4.77E-01	3.33E-01	<=	3.80E+00	WEIGHT
10	3.33E-01	-4.77E-01	3.33E-01	<=	3.80E+00	WEIGHT
11	3.33E-01	-4.77E-01	3.33E-01	<=	3.80E+00	WEIGHT
12	3.33E-01	-4.77E-01	3.33E-01	<=	3.80E+00	WEIGHT
13	3.33E-01	-4.77E-01	3.33E-01	<=	3.80E+00	WEIGHT
14	3.33E-01	-4.77E-01	3.33E-01	<=	3.80E+00	WEIGHT
15	3.33E-01	-4.77E-01	3.33E-01	<=	3.80E+00	WEIGHT
16	3.33E-01	-4.77E-01	3.33E-01	<=	3.80E+00	WEIGHT
17	3.33E-01	-4.77E-01	3.33E-01	<=	3.80E+00	WEIGHT

18	3.33E-01	-4.77E-01	3.33E-01	<=	3.80E+00	WEIGHT
19	3.33E-01	-4.77E-01	3.33E-01	<=	3.80E+00	WEIGHT
20	3.33E-01	-4.77E-01	3.33E-01	<=	3.80E+00	WEIGHT

Apart from the obvious, the optimized model's density and its reduction concerning the original design can be indirectly calculated. The necessary information can be exported to a CSV file. As mentioned above, this file contains density values of the elements indicating the type of lattice structures and the lower boundaries of the solid and lattice areas used. This data can be processed externally. The CSV file can be opened using a spreadsheet editor (e.g., Microsoft Excel). the data are processed first so that each cell contains only one price. The first column shows the number of each item as it is determined by the cellular structure process (Table 1). In the second column, the value of the optimal density that every element has is assigned. Therefore, it is enabled to calculate the number of elements and the summary of their densities to reduce the data to the desired results.

Table 2. Sparse Matrix Solver values

	Cycle		**Design Objective**		**Most critical cos-traint**	
	Value	Norm. Value	Resp. Value	Bound Type	Bound Value	Resp. Type
INITIAL	3.48E-01	-4.76E-01	3.48E-01	<=	3.80E+00	WEIGHT
1	3.33E-01	-4.77E-01	3.33E-01	<=	3.80E+00	WEIGHT
2	3.33E-01	-4.77E-01	3.33E-01	<=	3.80E+00	WEIGHT
3	3.33E-01	-4.77E-01	3.33E-01	<=	3.80E+00	WEIGHT
4	3.33E-01	-4.77E-01	3.33E-01	<=	3.80E+00	WEIGHT
5	3.33E-01	-4.77E-01	3.33E-01	<=	3.80E+00	WEIGHT
6	3.33E-01	-4.77E-01	3.33E-01	<=	3.80E+00	WEIGHT
7	3.33E-01	-4.77E-01	3.33E-01	<=	3.80E+00	WEIGHT
8	3.33E-01	-4.77E-01	3.33E-01	<=	3.80E+00	WEIGHT
9	3.33E-01	-4.77E-01	3.33E-01	<=	3.80E+00	WEIGHT
10	3.33E-01	-4.77E-01	3.33E-01	<=	3.80E+00	WEIGHT
11	3.33E-01	-4.77E-01	3.33E-01	<=	3.80E+00	WEIGHT
12	3.33E-01	-4.77E-01	3.33E-01	<=	3.80E+00	WEIGHT
13	3.33E-01	-4.77E-01	3.33E-01	<=	3.80E+00	WEIGHT
14	3.33E-01	-4.77E-01	3.33E-01	<=	3.80E+00	WEIGHT
15	3.33E-01	-4.77E-01	3.33E-01	<=	3.80E+00	WEIGHT
16	3.33E-01	-4.77E-01	3.33E-01	<=	3.80E+00	WEIGHT
17	3.33E-01	-4.77E-01	3.33E-01	<=	3.80E+00	WEIGHT
18	3.33E-01	-4.77E-01	3.33E-01	<=	3.80E+00	WEIGHT
19	3.33E-01	-4.77E-01	3.33E-01	<=	3.80E+00	WEIGHT
20	3.33E-01	-4.77E-01	3.33E-01	<=	3.80E+00	WEIGHT

This way, the density of the optimal model is calculated. Still, considering that the original model has a density equal to the unit for each of its elements, the corresponding value of the optimal design is quickly concluded.

The process was continued by going back into the modelling module within Simcenter 3D and importing the created STL file.

It was also enabled to open the design space geometry and then use Simcenter 3D geometry tools to trace the facet body's alignment and then cut the design space part until having the desired shape.

NX Nastran TO helps CAE analysts use advanced capabilities to execute design concept studies and determine the best shape to meet performance requirements.

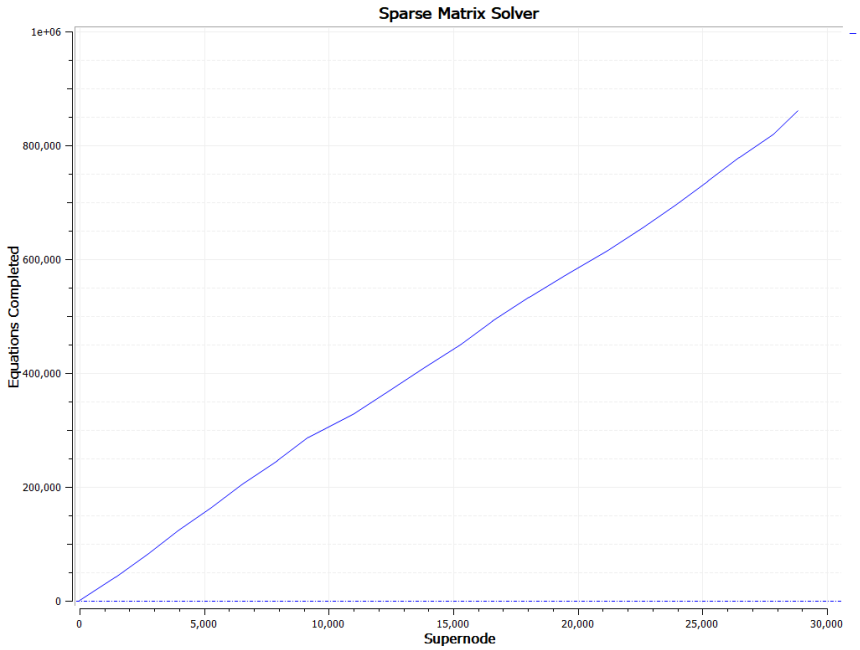

Figure 47.Sparse Matrix Solver

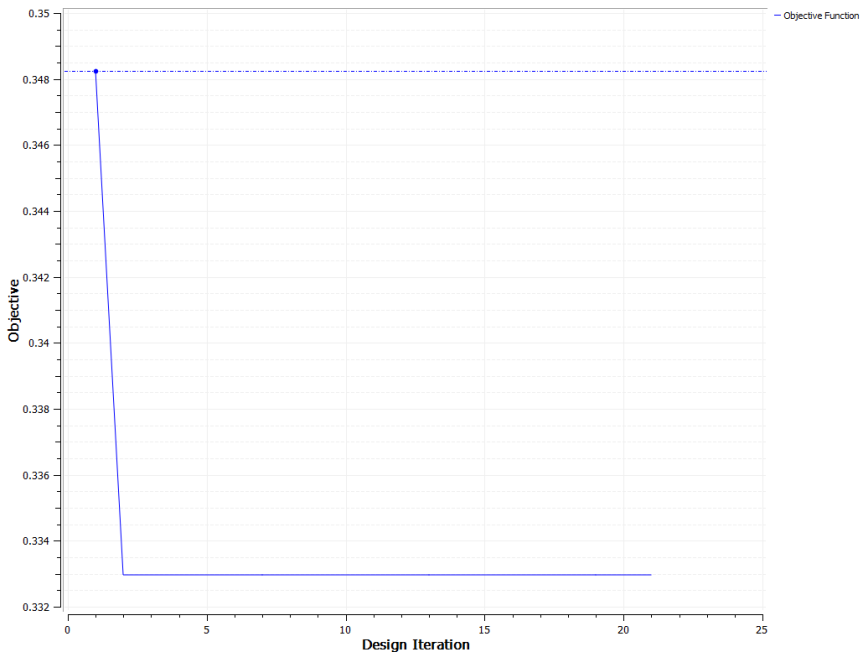

Figure 48. Objective Function capture

Table 3. Objective function values

Design Iteration	Objective Function
1	0.348245
2	0.332979
3	0.332976
4	0.332975
5	0.332974
6	0.332974
7	0.332974
8	0.332974
9	0.332973
10	0.332973
11	0.332973
12	0.332973
13	0.332973
14	0.332972
15	0.332973
16	0.332972
17	0.332973
18	0.332972
19	0.332973
20	0.332972
21	0.332973

And then, a verification solution was created.

4.2 Validation

When the TO was completed and the obtained results were presented graphically, the optimal solution should be checked. More specifically, it is necessary to check if the resulting optimal design satisfies the restrictions that have been set and generally to control its behaviour under boundary conditions. The results that can be used for this purpose are those that have not undergone any smoothing. Based on these, a verification solution is created. In essence, the verification solution is a copy of the original solution but contains only the data retained during the optimisation implementation.

Verification Solution → Create

Simulation Navigator → Copy of Solution 1 → Make Active

Copy of Solution 1 → Edit

In the new tab: Bulk Data → Maximum Number of Design Cycles (DESMAX), 0 value

Copy of Solution 1 → Solve

Uncheck the Model Setup Check and Solve

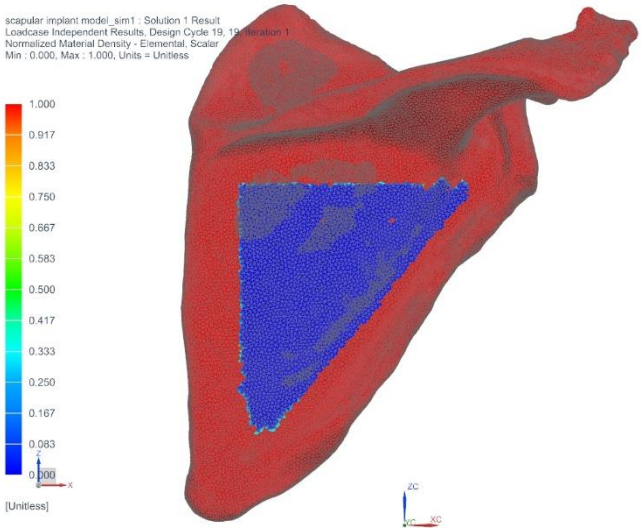

Figure 49. Load case independent results

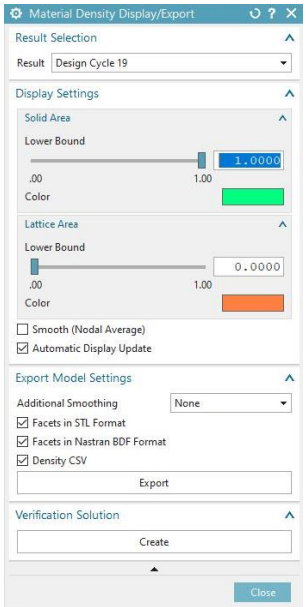

Figure 50. Validation solution material density results

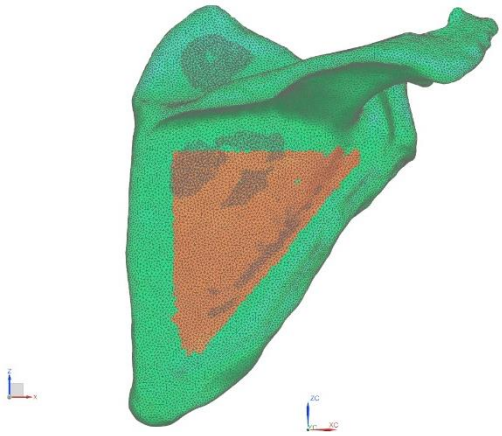

Figure 51. Validation solution material density results

Then the STL exported file for the material density results was imported back to convergent modelling environment and its geometry was followed for the creation of the TO model.

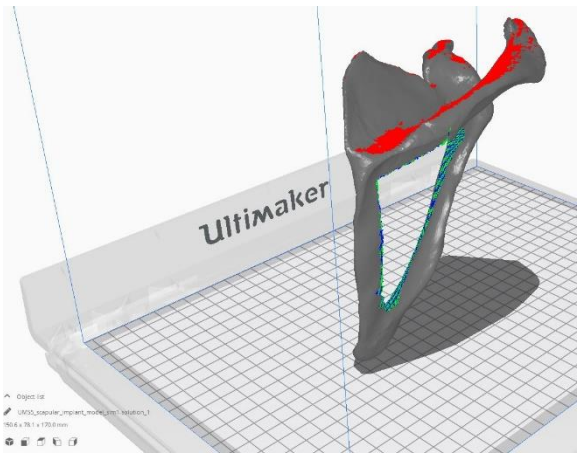

Figure 52. Smoothed STL exported and opened in slicing software 'Cura'

4.3 FEM results

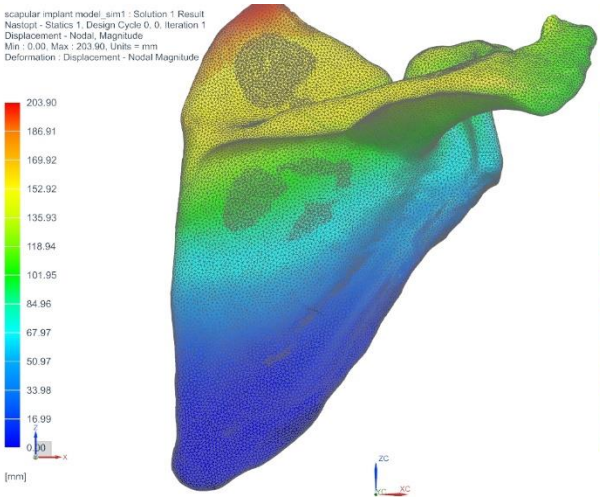

Figure 53. Displacement results

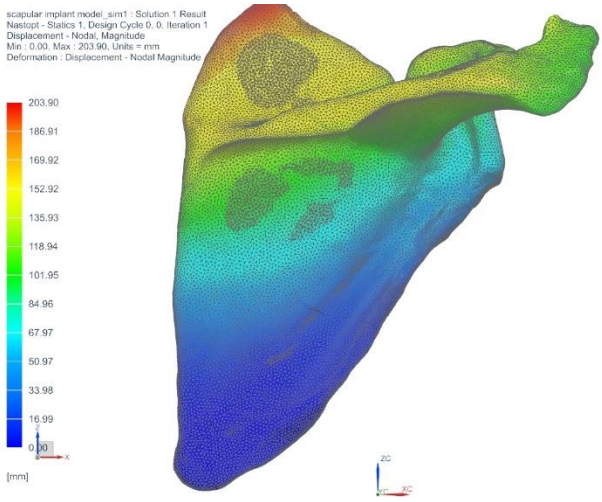

Figure 54. Stress results

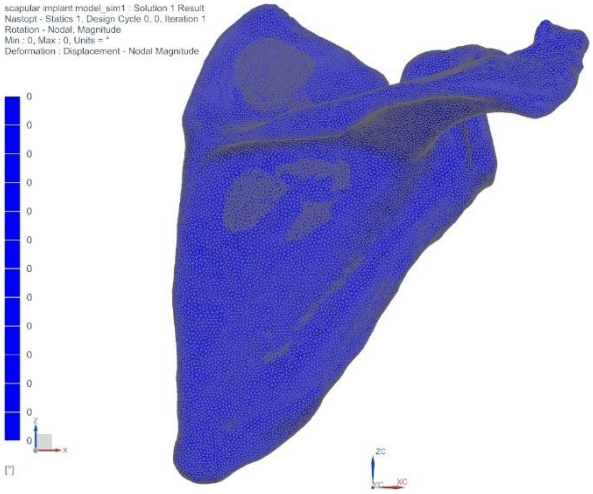

Figure 55. Rotation results

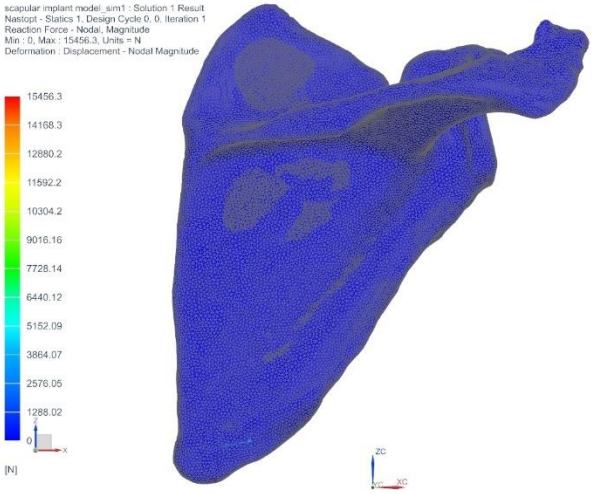

Figure 56. Reaction force results

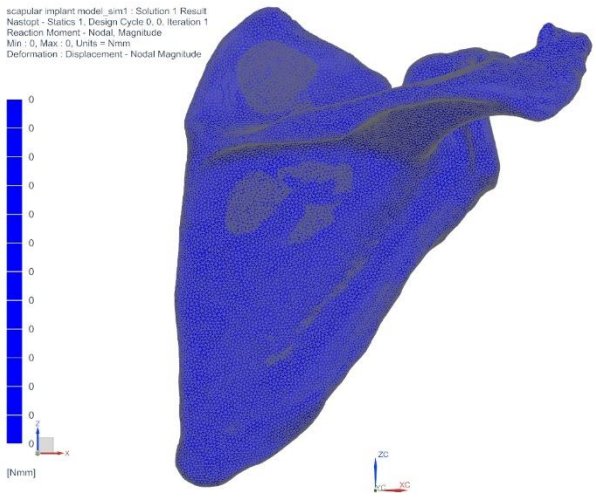

Figure 57. Reaction moment results

4.4 Lattice structure

Finally, lattice structures were applied to the model. So far, implant geometry was introduced in the NX software, and all problem parameters have been defined. Emphasis is given to the lattice structure type but also on the design constraint concerning the weight. Finally, the lattice structure was selected as the 'Octahedroid' because it has a great porosity percentage of 93%, while its stiffness in x and y vector equals to 52 and in z to 51.

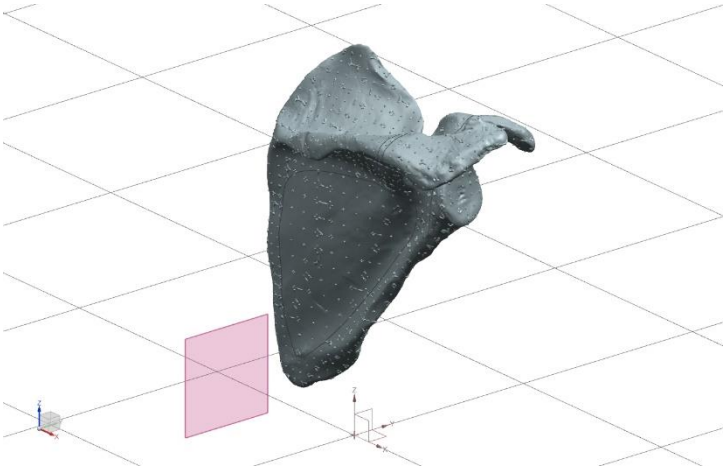

Figure 58. Octahedroid lattice structure application

4.5 Discussion and Future Work

Amputation remains the most common treatment for large tumours. However, other options such as the pelvis, clavicle and scapula salvage have become more popular. This can be attributed to advances in surgical technique, better preoperative imaging, more effective Neoadjuvant chemotherapy and improved preoperative imaging. In recent years, the development of customised titanium alloy prostheses has greatly improved limb salvage surgery.

This study describes the process of designing and manufacturing patient-specific implants using CT scan data, which usually takes a shorter time. Siemens NX software is utilised for the successful FE study and TO. The FEA tool can be used to solve complex problems. This eliminates the limitations of analytical and experimental approaches for stress analysis. Only simulation models were used in this study. However, the STL files are available to create and manipulate implant designs employing either direct or indirect methods. High-end additive manufacturing of implants can be expensive due to the use of costly software and machines. Direct manufacturing can be more expensive than indirect because of the low-end 3D printing technology used for prototyping. Open-source software is a great way to reduce the cost of the final implant. A combination of free software, low-cost 3D printers, and a quick tooling approach allows the user to produce patient-specific economical implants in a much shorter time. The additively produced patient-specific implant also decreases surgery time and patient recovery times while lowering the risk of implant failure in the future.

From the above results, it can be concluded that there are much more possibilities concerning the novel design prospect of a biomedical implant. This project was focused on the TO and the macro design perspective. However, numerous changes can occur if the micro design perspective is investigated. AM allows the designer/engineer to approach the design aspect from multiple aspects. For instance, it would be interesting to expand this implant's mechanical properties by manipulating the g-code needed for its manufacturing. Supposing this is possible, different stiffness or elasticity could be achieved in various model surfaces, and heterogeneity could be implemented using FGMs.

Another aspect that should be considered is the material's choice. So, materials that will be more biocompatible, like biomaterials, can be adopted, and materials that will have human cells, helping to regenerate the actual bone tissue. Drug-eluting materials are also promising and could be employed for in-situ 3D printing, helping the graft regenerate.

Bibliography

[1] A. Biazzo, M. De Paolis, and D. M. Donati, "Scapular reconstructions after resection for bone tumors: A single-institution experience and review of the literature," *Acta Biomed.*, vol. 89, no. 3, pp. 415–422, 2018, doi: 10.23750/abm.v89i3.5655.

[2] K. Hayashi *et al.*, "Functional outcomes after total scapulectomy for malignant bone or soft tissue tumors in the shoulder girdle," *Int. J. Clin. Oncol.*, vol. 16, no. 5, pp. 568–573, 2011, doi: 10.1007/s10147-011-0229-z.

[3] H. J. Mankin, M. C. Gebhardt, L. C. Jennings, D. S. Springfield, and W. W. Tomford, "Long-term results of allograft replacement in the management of bone tumors," *Clin. Orthop. Relat. Res.*, no. 324, pp. 86–97, 1996, doi: 10.1097/00003086-199603000-00011.

[4] E. Pala, G. Trovarelli, T. Calabrò, A. Angelini, C. N. Abati, and P. Ruggieri, "Survival of Modern Knee Tumor Megaprostheses: Failures, Functional Results, and a Comparative Statistical Analysis," *Clin. Orthop. Relat. Res.*, vol. 473, no. 3, pp. 891–899, 2015, doi: 10.1007/s11999-014-3699-2.

[5] B. Wang, Y. Hao, F. Pu, W. Jiang, and Z. Shao, "Computer-aided designed, three dimensional-printed hemipelvic prosthesis for peri-acetabular malignant bone tumour," *Int. Orthop.*, vol. 42, no. 3, pp. 687–694, 2018, doi: 10.1007/s00264-017-3645-5.

[6] E. R. Ahlmann, L. R. Menendez, C. Kermani, and H. Gotha, "Survivorship and clinical outcome of modular endoprosthetic reconstruction for neoplastic disease of the lower limb," *J. Bone Jt. Surg. - Ser. B*, vol. 88, no. 6, pp. 790–795, 2006, doi: 10.1302/0301-620X.88B6.17519.

[7] G. Niccoli, D. Mercurio, and F. Cortese, "Bone scan in painful knee arthroplasty: obsolete or actual examination?," *Acta Bio Medica Atenei Parm.*, vol. 88, no. 2-S, pp. 68–77, 2017, doi: 10.23750/abm.v88i2.

[8] E. N. Zeegen, L. A. Aponte-Tinao, F. J. Hornicek, M. C. Gebhardt, and H. J. Mankin, "Survivorship Analysis of 141 Modular Metallic Endoprostheses at Early Followup," *Clin. Orthop. Relat. Res.*, no. 420, pp. 239–250, 2004, doi: 10.1097/00003086-200403000-00034.

[9] C. Quental, J. Folgado, P. R. Fernandes, and J. Monteiro, "Subject-specific bone remodelling of the scapula," *Computer Methods in Biomechanics and Biomedical Engineering*, vol. 17, no. 10. Taylor & Francis, pp. 1129–1143, 2014, doi: 10.1080/10255842.2012.738198.

[10] K. Hayashi *et al.*, "Experience of total scapular excision for musculoskeletal tumor and reconstruction in eastern Asian countries," *J. Bone Oncol.*, vol. 9, no. October 2016, pp. 55–58, 2017, doi: 10.1016/j.jbo.2016.10.003.

[11] M. J. Harvey and H. G. Rosenthal, "Reconstruction with Total Scapular Reverse Total Shoulder Endoprosthesis after Radical Tumor Excision," *Case Rep. Oncol. Med.*, vol. 2021, pp. 1–7, 2021, doi: 10.1155/2021/1968621.

[12] T. Ji, W. Guo, R. L. Yang, X. D. Tang, and Y. F. Wang, "Modular hemipelvic endoprosthesis reconstruction-Experience in 100 patients with mid-term follow-up results," *Eur. J. Surg. Oncol.*, vol. 39, no. 1, pp. 53–60, 2013, doi: 10.1016/j.ejso.2012.10.002.

[13] W. Sun, J. Li, Q. Li, G. Li, and Z. Cai, "Clinical Effectiveness of Hemipelvic Reconstruction

Using Computer-Aided Custom-Made Prostheses After Resection of Malignant Pelvic Tumors," *J. Arthroplasty*, vol. 26, no. 8, pp. 1508–1513, 2011, doi: 10.1016/j.arth.2011.02.018.

[14] A. Abudu, R. J. Grimer, S. R. Cannon, S. R. Carter, and R. S. Sneath, "Reconstruction of the hemipelvis after the excision of malignant tumours," *J. Bone Jt. Surg. - Ser. B*, vol. 79, no. 5, pp. 773–779, 1997, doi: 10.1302/0301-620X.79B5.6749.

[15] S. L. Sing, J. An, W. Y. Yeong, and F. E. Wiria, "Laser and electron-beam powder-bed additive manufacturing of metallic implants: A review on processes, materials and designs," *J. Orthop. Res.*, vol. 34, no. 3, pp. 369–385, 2016, doi: 10.1002/jor.23075.

[16] P. Xiu *et al.*, "Tailored Surface Treatment of 3D Printed Porous Ti6Al4V by Microarc Oxidation for Enhanced Osseointegration via Optimized Bone In-Growth Patterns and Interlocked Bone/Implant Interface," *ACS Appl. Mater. Interfaces*, vol. 8, no. 28, pp. 17964–17975, 2016, doi: 10.1021/acsami.6b05893.

[17] F. A. Shah, A. Snis, A. Matic, P. Thomsen, and A. Palmquist, "3D printed Ti6Al4V implant surface promotes bone maturation and retains a higher density of less aged osteocytes at the bone-implant interface," *Acta Biomater.*, vol. 30, pp. 357–367, 2016, doi: 10.1016/j.actbio.2015.11.013.

[18] J. W. Park, H. G. Kang, K. M. Lim, J. H. Kim, and H. S. Kim, "Three-Dimensionally Printed Personalized Implant Design and Reconstructive Surgery for a Bone Tumor of the Calcaneus: A Case Report," *JBJS case Connect.*, vol. 8, no. 2, p. e25, 2018, doi: 10.2106/JBJS.CC.17.00212.

[19] J. L. Mulhern, N. M. Protzman, A. M. White, and S. A. Brigido, "Salvage of Failed Total Ankle Replacement Using a Custom Titanium Truss," *J. Foot Ankle Surg.*, vol. 55, no. 4, pp. 868–873, 2016, doi: 10.1053/j.jfas.2015.12.011.

[20] K. R. Dai, M. N. Yan, Z. A. Zhu, and Y. H. Sun, "Computer-Aided Custom-Made Hemipelvic Prosthesis Used in Extensive Pelvic Lesions," *J. Arthroplasty*, vol. 22, no. 7, pp. 981–986, 2007, doi: 10.1016/j.arth.2007.05.002.

[21] H. Li, X. Qu, Y. Mao, K. Dai, and Z. Zhu, "Custom Acetabular Cages Offer Stable Fixation and Improved Hip Scores for Revision THA With Severe Bone Defects," *Clin. Orthop. Relat. Res.*, vol. 474, no. 3, pp. 731–740, 2016, doi: 10.1007/s11999-015-4587-0.

[22] C. C. Berasi, K. R. Berend, J. B. Adams, E. L. Ruh, and A. V. Lombardi, "Are Custom Triflange Acetabular Components Effective for Reconstruction of Catastrophic Bone Loss?," *Clin. Orthop. Relat. Res.*, vol. 473, no. 2, pp. 528–535, 2015, doi: 10.1007/s11999-014-3969-z.

[23] H. Liang, T. Ji, Y. Zhang, Y. Wang, and W. Guo, "Reconstruction with 3D-printed pelvic endoprostheses after resection of a pelvic tumour," *Bone Jt. J.*, vol. 99-B, no. 2, pp. 267–275, 2017, doi: 10.1302/0301-620X.99B2.BJJ-2016-0654.R1.

[24] R. J. Mobbs, M. Coughlan, R. Thompson, C. E. Sutterlin, and K. Phan, "The utility of 3D printing for surgical planning and patient-specific implant design for complex spinal pathologies: Case report," *J. Neurosurg. Spine*, vol. 26, no. 4, pp. 513–518, 2017, doi: 10.3171/2016.9.SPINE16371.

[25] H. Fan *et al.*, "Implantation of customized 3-D printed titanium prosthesis in limb salvage surgery: A case series and review of the literature," *World J. Surg. Oncol.*, vol. 13, no. 1, pp. 1–10, 2015, doi: 10.1186/s12957-015-0723-2.

[26] J. Y. Lee, J. An, and C. K. Chua, "Fundamentals and applications of 3D printing for novel materials," *Appl. Mater. Today*, vol. 7, pp. 120–133, 2017, doi: 10.1016/j.apmt.2017.02.004.

[27] J. Y. Lee, J. An, and C. K. Chua, "Fundamentals and applications of 3D printing for novel

materials," *Appl. Mater. Today*, vol. 7, pp. 120–133, 2017, doi: 10.1016/j.apmt.2017.02.004.

[28] L. E. J. Thomas-Seale, J. C. Kirkman-Brown, M. M. Attallah, D. M. Espino, and D. E. T. Shepherd, "The barriers to the progression of additive manufacture: Perspectives from UK industry," *Int. J. Prod. Econ.*, vol. 198, no. February, pp. 104–118, 2018, doi: 10.1016/j.ijpe.2018.02.003.

[29] A. Angelini, D. Kotrych, G. Trovarelli, A. Szafrański, A. Bohatyrewicz, and P. Ruggieri, "Analysis of principles inspiring design of three-dimensional-printed custom-made prostheses in two referral centres," *Int. Orthop.*, vol. 44, no. 5, pp. 829–837, 2020, doi: 10.1007/s00264-020-04523-y.

[30] A. Ghilan, A. P. Chiriac, L. E. Nita, A. G. Rusu, I. Neamtu, and V. M. Chiriac, "Trends in 3D Printing Processes for Biomedical Field: Opportunities and Challenges," *J. Polym. Environ.*, vol. 28, no. 5, pp. 1345–1367, 2020, doi: 10.1007/s10924-020-01722-x.

[31] J. Ni *et al.*, "Three-dimensional printing of metals for biomedical applications," *Mater. Today Bio*, vol. 3, no. August, 2019, doi: 10.1016/j.mtbio.2019.100024.

[32] "Specification for additive manufacturing file format (AMF)." https://www.astm.org/f2915-20.html.

[33] "ISO/ASTM 52915:2016 Specification for additive manufacturing file format." https://www.iso.org/standard/67472.html.

[34] "Additive manufacturing file format." https://en.wikipedia.org/wiki/Additive_manufacturing_file_format#cite_note-ASTM_F2915-1.

[35] "3MF Consortium." https://3mf.io/.

[36] "What is 3mf?" https://web.archive.org/web/20191209133517/https://3mf.io/what-is-3mf/.

[37] "About Us." https://web.archive.org/web/20191010054235/https://3mf.io/about-us/.

[38] "Adoption." https://3mf.io/adoption/.

[39] C. Specification and R. Guide, "3D Manufacturing Format About this Specification," pp. 1–32, 2021, [Online]. Available: https://github.com/3MFConsortium/spec_core/releases/download/1.2.3/3MF_Core_Specification_v1_2_3.pdf.

[40] D. V. Smith *et al.*, "Evaluation of the Medical Diagnostic Imaging Support system based on 2 years of clinical experience," *J. Digit. Imaging*, vol. 8, no. 2, pp. 75–87, 1995, doi: 10.1007/BF03168130.

[41] D. E. Best, S. C. Horii, W. C. Bennett, and C. R. Parisot, "<title>Update of the ACR-NEMA digital imaging and communications in medicine standard</title>," *Med. Imaging VI PACS Des. Eval.*, vol. 1654, pp. 356–361, 1992, doi: 10.1117/12.60322.

[42] "SearchHealthIT." https://searchhealthit.techtarget.com/definition/DICOM-Digital-Imaging-and-Communications-in-Medicine.

[43] E. C. D. Clunie, "Digital Imaging and Communications in Medicine (DICOM) - Application/dicom MIME Sub-type Registration," *Kaos GL Derg.*, vol. 2, no. 75, pp. 147–173, 2002.

[44] Y. K. Modi and S. Sanadhya, "Design and additive manufacturing of patient-specific cranial and pelvic bone implants from computed tomography data," *J. Brazilian Soc. Mech. Sci. Eng.*, vol. 40, no. 10, pp. 1–11, 2018, doi: 10.1007/s40430-018-1425-9.

[45] A. Haleem and M. Javaid, "Role of CT and MRI in the design and development of orthopaedic

model using additive manufacturing," *J. Clin. Orthop. Trauma*, vol. 9, no. 3, pp. 213–217, 2018, doi: 10.1016/j.jcot.2018.07.002.

[46] S. Kanagalingam, D. Shepherd, M. Fernandez-Vicente, D. Wimpenny, and L. Thomas-Seale, "Design principles to increase the patient specificity of high tibial osteotomy fixation devices," *Proc. Int. Conf. Eng. Des. ICED*, vol. 2019-Augus, no. AUGUST, pp. 917–926, 2019, doi: 10.1017/dsi.2019.96.

[47] F. M. Cross, Sarah J. Linker, Kay E. Leslie, "The Recent Revolution in the Design and Manufacture of Cranial Implants: Modern Advancements and Future Directions," *Physiol. Behav.*, vol. 176, no. 1, pp. 100–106, 2016, doi: 10.1227/NEU.0000000000000899.The.

[48] J. T. Tuomi *et al.*, "In vitro cytotoxicity and surface topography evaluation of additive manufacturing titanium implant materials," *J. Mater. Sci. Mater. Med.*, vol. 28, no. 3, 2017, doi: 10.1007/s10856-017-5863-1.

[49] W. R. Lacefield, "UNCOATED / CERAMIC-COATED IMPLANT MATERIALS," pp. 21–26, 1999.

[50] L. Lü, J. Y. H. Fuh, and Y. S. Wong, "Selective Laser Sintering," *Laser-Induced Mater. Process. Rapid Prototyp.*, pp. 89–142, 2001, doi: 10.1007/978-1-4615-1469-5_5.

[51] B. Gadagi and R. Lekurwale, "A review on advances in 3D metal printing," *Mater. Today Proc.*, vol. 45, pp. 277–283, 2020, doi: 10.1016/j.matpr.2020.10.436.

[52] P. K. Gokuldoss, S. Kolla, and J. Eckert, "Additive manufacturing processes: Selective laser melting, electron beam melting and binder jetting-selection guidelines," *Materials (Basel).*, vol. 10, no. 6, 2017, doi: 10.3390/ma10060672.

[53] A. H. Chern *et al.*, "Build orientation, surface roughness, and scan path influence on the microstructure, mechanical properties, and flexural fatigue behavior of Ti–6Al–4V fabricated by electron beam melting," *Mater. Sci. Eng. A*, vol. 772, no. November 2019, p. 138740, 2020, doi: 10.1016/j.msea.2019.138740.

[54] V. Lunetto, M. Galati, L. Settineri, and L. Iuliano, "Unit process energy consumption analysis and models for Electron Beam Melting (EBM): Effects of process and part designs," *Addit. Manuf.*, vol. 33, no. November 2019, p. 101115, 2020, doi: 10.1016/j.addma.2020.101115.

[55] D. G. Ahn, *Directed Energy Deposition (DED) Process: State of the Art*, vol. 8, no. 2. Korean Society for Precision Engineering, 2021.

[56] S. L. Sing, C. F. Tey, J. H. K. Tan, S. Huang, and W. Y. Yeong, *3D printing of metals in rapid prototyping of biomaterials: Techniques in additive manufacturing*, Second Edi. Elsevier Ltd., 2019.

[57] S. L. Sing, C. F. Tey, J. H. K. Tan, S. Huang, and W. Y. Yeong, *3D printing of metals in rapid prototyping of biomaterials: Techniques in additive manufacturing*, Second Edi. Elsevier Ltd., 2019.

[58] A. Ramakrishnan and G. P. Dinda, "Direct laser metal deposition of Inconel 738," *Mater. Sci. Eng. A*, vol. 740–741, no. October 2018, pp. 1–13, 2019, doi: 10.1016/j.msea.2018.10.020.

[59] D. Shamvedi, C. Danilenkoff, S. Karam, P. O'Leary, and R. Raghavendra, "3D printed periodic structures in a horn antenna for side-lobe reduction using direct metal laser sintering," *IET Conf. Publ.*, vol. 2017, no. CP732, pp. 3–6, 2017, doi: 10.1049/cp.2017.0244.

[60] D. Jafari, W. W. Wits, and B. J. Geurts, "Metal 3D-printed wick structures for heat pipe application: Capillary performance analysis," *Appl. Therm. Eng.*, vol. 143, no. July, pp. 403–414, 2018, doi: 10.1016/j.applthermaleng.2018.07.111.

[61] S. M. Yusuf and N. Gao, "Influence of energy density on metallurgy and properties in metal

additive manufacturing," *Mater. Sci. Technol. (United Kingdom)*, vol. 33, no. 11, pp. 1269–1289, 2017, doi: 10.1080/02670836.2017.1289444.

[62] A. Zemmari and J. Benois-Pineau, "Optimization methods," *SpringerBriefs Comput. Sci.*, pp. 21–33, 2020, doi: 10.1007/978-3-030-34376-7_4.

[63] M. Zhou, N. Pagaldipti, H. L. Thomas, and Y. K. Shyy, "An integrated approach to topology, sizing, and shape optimization," *Struct. Multidiscip. Optim.*, vol. 26, no. 5, pp. 308–317, 2004, doi: 10.1007/s00158-003-0351-2.

[64] G. G. Tejani, V. J. Savsani, V. K. Patel, and P. V. Savsani, "Size, shape, and topology optimization of planar and space trusses using mutation-based improved metaheuristics," *J. Comput. Des. Eng.*, vol. 5, no. 2, pp. 198–214, 2018, doi: 10.1016/j.jcde.2017.10.001.

[65] L. Giovannelli, J. J. Ródenas, J. M. Navarro-Jiménez, and M. Tur, "Direct medical image-based Finite Element modelling for patient-specific simulation of future implants," *Finite Elem. Anal. Des.*, vol. 136, no. July, pp. 37–57, 2017, doi: 10.1016/j.finel.2017.07.010.

[66] I. P. Rosinha, K. V. Gernaey, J. M. Woodley, and U. Krühne, "Topology optimization for biocatalytic microreactor configurations," *Comput. Aided Chem. Eng.*, vol. 37, no. June, pp. 1463–1468, 2015, doi: 10.1016/B978-0-444-63577-8.50089-9.

[67] Y. Sui and X. Peng, *Foundation of the ICM (independent, continuous and mapping) method*. 2018.

[68] A. W. Gebisa and H. G. Lemu, "A case study on topology optimized design for additive manufacturing," *IOP Conf. Ser. Mater. Sci. Eng.*, vol. 276, no. 1, 2017, doi: 10.1088/1757-899X/276/1/012026.

[69] O. Sigmund and K. Maute, "Topology optimization approaches: A comparative review," *Struct. Multidiscip. Optim.*, vol. 48, no. 6, pp. 1031–1055, 2013, doi: 10.1007/s00158-013-0978-6.

[70] Q. Guo, W. Yao, W. Li, and N. Gupta, "Constitutive models for the structural analysis of composite materials for the finite element analysis: A review of recent practices," *Compos. Struct.*, vol. 260, no. June 2020, p. 113267, 2021, doi: 10.1016/j.compstruct.2020.113267.

[71] M. Zhou and G. I. N. Rozvany, "DCOC: An optimality criteria method for large systems Part II: Algorithm," *Struct. Optim.*, vol. 6, no. 4, pp. 250–262, 1993, doi: 10.1007/BF01743384.

[72] G. I. N. Rozvany, "A critical review of established methods of structural topology optimization," *Struct. Multidiscip. Optim.*, vol. 37, no. 3, pp. 217–237, 2009, doi: 10.1007/s00158-007-0217-0.

[73] N. Olhoff and J. E. Taylor, "On structural optimization," *J. Appl. Mech. Trans. ASME*, vol. 50, no. 4, pp. 1139–1151, 1983, doi: 10.1115/1.3167196.

[74] G. H. Yoon, Y. Y. Kim, M. P. Bendsøe, and O. Sigmund, "Hinge-free topology optimization with embedded translation-invariant differentiate wavelet shrinkage," *Struct. Multidiscip. Optim.*, vol. 27, no. 3, pp. 139–150, 2004, doi: 10.1007/s00158-004-0378-z.

[75] M. P. Bendsøe, "Optimal shape design as a material distribution problem," *Struct. Optim.*, vol. 1, no. 4, pp. 193–202, 1989, doi: 10.1007/BF01650949.

[76] G. Allaire, F. Jouve, and A. M. Toader, *Structural optimization using sensitivity analysis and a level-set method*, vol. 194, no. 1. 2004.

[77] C. Mattheck, "Engineering Components grow like trees," *Materwiss. Werksttech.*, vol. 21, no. 4, pp. 143–168, 1990, doi: 10.1002/mawe.19900210403.

[78] Q. Li, G. P. Steven, and Y. M. Xie, "A simple checkerboard suppression algorithm for

evolutionary structural optimization," *Struct. Multidiscip. Optim.*, vol. 22, no. 3, pp. 230–239, 2001, doi: 10.1007/s001580100140.

[79] J. Martínez-Frutos and D. Herrero-Pérez, "Evolutionary topology optimization of continuum structures under uncertainty using sensitivity analysis and smooth boundary representation," *Comput. Struct.*, vol. 205, pp. 15–27, 2018, doi: 10.1016/j.compstruc.2018.05.003.

[80] M. Sotola, P. Marsalek, D. Rybansky, M. Fusek, and D. Gabriel, "Sensitivity analysis of key formulations of topology optimization on an example of cantilever bending beam," *Symmetry (Basel).*, vol. 13, no. 4, pp. 1–25, 2021, doi: 10.3390/sym13040712.

[81] C. Wang, N. Huang, Y. Bai, and S. Zhang, "A method of network topology optimization design considering application process characteristic," *Mod. Phys. Lett. B*, vol. 32, no. 7, pp. 1–11, 2018, doi: 10.1142/S0217984918500914.

[82] J. Brennan and K. Hayes, "Recent applications of topology and topography optimization in automotive design," *8th Symp. Multidiscip. Anal. Optim.*, no. September, 2000, doi: 10.2514/6.2000-4709.

[83] "NX Nastran Topology Optimization in Simcenter." https://docs.plm.automation.siemens.com/data_services/resources/nxnastran/11/help/common/en_US/graphics/fileLibrary/nastran/nastran_nonXPS/simcenter_top_opt/simcenter_top_opt.pdf.

[84] "Topology optimization workflow." https://docs.plm.automation.siemens.com/tdoc/nx/12/nx_help#uid:xid1128419:index_advanced:xid384581:xid1331664:xid1323082.

[85] "Solution dialog box (NX Nastran), Bulk Data page." https://docs.plm.automation.siemens.com/tdoc/nx/12/nx_help#uid:id632436.

[86] D. Kang, S. Park, Y. Son, S. Yeon, S. H. Kim, and I. Kim, "Multi-lattice inner structures for high-strength and light-weight in metal selective laser melting process," *Mater. Des.*, vol. 175, p. 107786, 2019, doi: 10.1016/j.matdes.2019.107786.

[87] T. Maconachie *et al.*, "SLM lattice structures: Properties, performance, applications and challenges," *Mater. Des.*, vol. 183, p. 108137, 2019, doi: 10.1016/j.matdes.2019.108137.

[88] Y. Tang and Y. F. Zhao, "A survey of the design methods for additive manufacturing to improve functional performance," *Rapid Prototyp. J.*, vol. 22, no. 3, pp. 569–590, 2016, doi: 10.1108/RPJ-01-2015-0011.

[89] "Cults." https://cults3d.com/en.

[90] E. Maravelakis, K. David, A. Antoniadis, A. Manios, N. Bilalis, and Y. Papaharilaou, "Reverse engineering techniques for cranioplasty: A case study," *J. Med. Eng. Technol.*, vol. 32, no. 2, pp. 115–121, 2008, doi: 10.1080/03091900600700749.

[91] Y. Li *et al.*, "A Review on Functionally Graded Materials and Structures via Additive Manufacturing: From Multi-Scale Design to Versatile Functional Properties," *Adv. Mater. Technol.*, vol. 5, no. 6, 2020, doi: 10.1002/admt.201900981.

[92] H. Hibi, M. Ueda, and S. Torii, "Titanium implant in a vascularised scapular bone graft after a 6-year loading period," *Asian J. Oral Maxillofac. Surg.*, vol. 20, no. 3, pp. 148–151, 2008, doi: 10.1016/S0915-6992(08)80037-4.

[93] N. Mitsuo, "Mechanical properties of biomedical titanium alloys," *Mater. Sci. Eng. A*, vol. 243, no. 1–2, pp. 231–236, 1998, [Online]. Available: http://www.sciencedirect.com/science/article/pii/S092150939700806X.

[94] J. Imanishi and P. F. M. Choong, "Three-dimensional printed calcaneal prosthesis following

total calcanectomy," *International Journal of Surgery Case Reports*, vol. 10. pp. 83–87, 2015, doi: 10.1016/j.ijscr.2015.02.037.

[95] D. McCutchen, E. Dibble, and M. M. Blount, "Phonemic effects in reading comprehension and text memory," *Appl. Cogn. Psychol.*, vol. 8, no. 6, pp. 597–611, 1994, doi: 10.1002/acp.2350080606.

[96] C. Hindorf, G. Glatting, C. Chiesa, O. Lindén, and G. Flux, "EANM dosimetry committee guidelines for bone marrow and whole-body dosimetry," *Eur. J. Nucl. Med. Mol. Imaging*, vol. 37, no. 6, pp. 1238–1250, 2010, doi: 10.1007/s00259-010-1422-4.

[97] "Meltio M450 Technical Datasheet." [Online]. Available: https://meltio3d.com/wp-content/uploads/2021/07/MeltioM450_TechnicalDatasheet_v2.3.pdf.

[98] L. Pelzer and C. Hopmann, "Additive manufacturing of non-planar layers with variable layer height," *Addit. Manuf.*, vol. 37, no. November 2020, p. 101697, 2021, doi: 10.1016/j.addma.2020.101697.

[99] C. Greer *et al.*, "Introduction to the design rules for Metal Big Area Additive Manufacturing," *Addit. Manuf.*, vol. 27, no. November 2018, pp. 159–166, 2019, doi: 10.1016/j.addma.2019.02.016.

[100] R. M. Paine and M. Voight, "The role of the scapula," *J. Orthop. Sports Phys. Ther.*, vol. 18, no. 1, pp. 386–391, 1993, doi: 10.2519/jospt.1993.18.1.386.

[101] "Winged Scapula | Serratus Anterior." https://nielasher.com/blogs/video-blog/massage-therapy-treating-winged-scapula.

[102] N. H. Hart, S. Nimphius, T. Rantalainen, A. Ireland, A. Siafarikas, and R. U. Newton, "Mechanical basis of bone strength: Influence of bone material, bone structure and muscle action," *J. Musculoskelet. Neuronal Interact.*, vol. 17, no. 3, pp. 114–139, 2017.

[103] F. Colas, J. Nevoux, and O. Gagey, "The subscapular and subcoracoid bursae: Descriptive and functional anatomy," *J. Shoulder Elb. Surg.*, vol. 13, no. 4, pp. 454–458, 2004, doi: 10.1016/j.jse.2004.02.001.